Table 3
Summary: GNP model validation study.

Test chemical	*gpt* assay	Histopathological analysis of preneoplastic lesions	Classification
AA	+	+	Genotoxic carcinogen
PDP	–	+	Nongenotoxic
PBZ	–	+	carcinogen
DL	–	–	Noncarcinogen

with DL did not increase the MFs of *gpt* delta rats and did not affect the development of preneoplastic lesions in the kidney, in line with the observation that DL is not carcinogenic in female rats. Moreover, there were no hyaline droplets indicating accumulation of α_{2u}-globulin in the proximal tubular epithelium. α_{2u}-Globulin-mediated renal carcinogenesis is not thought to be relevant in humans (Hard, 1998; Doi et al., 2007). However, these false-positive results in terms of human risk assessment can be avoided in the GNP model using female rats. Overall, our validation study demonstrated that the GNP model could be a valid tool to detect renal carcinogens and provide a variety of results and insights regarding the mechanisms underlying carcinogenesis (Table 3).

In conclusion, we have established a new medium-term *gpt* delta rat model for predicting chemicals with renal carcinogenicity; we termed this model the GNP model. Based on the results of our validation studies, we propose that the GNP model may represent a reliable system for analysis of chemical renal carcinogenicity and the underlying mode of action.

Conflict of interest

The authors declare that there are no conflicts of interest. K. M. is an employee of Otsuka Pharmaceutical Co., Ltd.

Acknowledgments

We appreciate the expert technical assistance of Ms. Ayako Kaneko and Ms. Yoshimi Komatsu. This work was supported by a Grant-in-Aid for Research on Food Sanitation from the Ministry of Health, Labor, and Welfare of Japan (H-24-shokuhin-ippan-012).

References

Athar M, Iqbal M. Ferric nitrilotriacetate promotes *N*-diethylnitrosamine-induced renal tumorigenesis in the rat: implications for the involvement of oxidative stress. Carcinogenesis 1998;19:1133–9.

Charles D, Leonard A. Mutagenicity tests with phenylbutazone in mammals. Toxicol Lett 1978;2:225–30.

Choudhary D, Jansson I, Stoilov I, Sarfarazi M, Schenkman JB. Expression patterns of mouse and human CYP orthologs (families 1–4) during development and in different adult tissues. Arch Biochem Biophys 2005;436:50–61.

Cohen SM, Arnold LL. Chemical carcinogenesis. Toxicol Sci 2011;120:S76–92.

Dietrich DR, Swenberg JA. Preneoplastic lesions in rodent kidney induced spontaneously or by non-genotoxic agents: predictive nature and comparison to lesions induced by genotoxic carcinogens. Mutat Res 1991a;248:239–60.

Dietrich DR, Swenberg JA. The presence of alpha 2u-globulin is necessary for *d*-limonene promotion of male rat kidney tumors. Cancer Res 1991b;51:3512–21.

Doi AM, Hill G, Seely J, Hailey JR, Kissling G, Bucher JR. Alpha 2u-globulin nephropathy and renal tumors in national toxicology program studies. Toxicol Pathol 2007;35:533–40.

Gebhart E, Wissmüller HF. Investigations on the effect of phenylbutazone on chromosomes and mitosis in the bone marrow of rats. Mutat Res 1973;17:283–6.

Goyer RA, Falk HL, Hogan M, Feldman DD, Richter W. Renal tumors in rats given trisodium nitrilotriacetic acid in drinking water for 2 years. J Natl Cancer Inst 1981;66:869–80.

Hard GC. Mechanisms of chemically induced renal carcinogenesis in the laboratory rodent. Toxicol Pathol 1998;26:104–12.

Hiasa Y, Konishi N, Nakaoka S, Nakamura T, Nishii K, Ohshima M. Promoting effects of potassium dibasic phosphate on early-stage renal carcinogenesis in unilaterally nephrectomized rats treated with *N*-ethyl-*N*-hydroxyethylnitrosamine. Jpn J Cancer Res 1992;83:688–94.

International Conference on Harmonisation (ICH). Testing for carcinogenicity of pharmaceuticals. ICH harmonized tripartite guideline 1997; 1997, Available from URL (http://www.ich.org/fileadmin/Public_Web_Site/ICH_Products/Guidelines/Safety/S1B/Step4/S1B_Guideline.pdf) (cited 1 August 2014) (Jul; S1 (B)).

Ishii Y, Takasu S, Kuroda K, Matsushita K, Kijima A, Nohmi T, et al. Combined application of comprehensive analysis for DNA modification and reporter gene mutation assay to evaluate kidneys of *gpt* delta rats given madder color or its constituents. Anal Bioanal Chem 2014;406:2467–75.

Ito N, Tamano S, Shirai T. A medium-term rat liver bioassay for rapid *in vivo* detection of carcinogenic potential of chemicals. Cancer Sci 2003;94:3–8.

Kakehashi A, Wei M, Fukushima S, Wanibuchi H. Oxidative stress in the carcinogenicity of chemical carcinogens. Cancers 2013;5:1332–54.

Kawamura Y, Hayashi H, Tajima O, Yamada S, Takayanagi T, Hori H, et al. Evaluation of the genotoxicity of aristolochic acid in the kidney and liver of F344 *gpt* delta transgenic rat using a 28-day repeated-dose protocol: a collaborative study of the *gpt* delta transgenic rat mutation assay. Genes Environ 2012;34:18–24.

Kari F, Bucher J, Haseman J, Eustis S, Huff J. Long-term exposure to the anti-inflammatory agent phenylbutazone induces kidney tumors in rats and liver tumors in mice. Jpn J Cancer Res 1995;86:252–63.

Kobayashi K, Mutai M, Goto K, Inada K, Tsukamoto T, Nakanishi H, et al. Effects of carbon tetrachloride administration on initiation of liver cell foci by the non-hepatocarcinogens *N*-methyl-*N'*-nitro-*N*-nitrosoguanidine (MNNG) and benzo(*a*)pyrene (B(a)P). Cancer Lett 1997;118:55–60.

Konishi N, Kitamura M, Hayashi I, Matsuda H, Tao M, Naitoh H, et al. Effect of methimazole on rat renal carcinogenesis induced by *N*-ethyl-*N*-hydroxyethylnitrosamine. Toxicol Pathol 1995;23:606–11.

Kuroda K, Ishii Y, Takasu S, Kijima A, Matsushita K, Watanabe M, et al. Cell cycle progression, but not genotoxic activity, mainly contributes to citrinin-induced renal carcinogenesis. Toxicology 2013;311:216–24.

Machemer L, Hess R. Comparative dominant lethal studies with phenylbutazone, thio-TEPA and MMS in the mouse. Experientia 1971;27:1050–2.

Maekawa A, Onodera H, Tanigawa H, Furuta K, Kanno J, Matsuoka C, et al. Long-term studies on carcinogenicity and promoting effect of phenylbutazone in DONRYU rats. J Natl Cancer Inst 1987;79:577–84.

Matsushita K, Kijima A, Ishii Y, Takasu S, Jin M, Kuroda K, et al. Development of a medium-term animal model using *gpt* delta rats to evaluate chemical carcinogenicity and genotoxicity. J Toxicol Pathol 2013;26:19–27.

Matsushita K, Kuroda K, Ishii Y, Takasu S, Kijima A, Hiroaki Kawaguchi, et al. Improvement and validation of a medium-term *gpt* delta rat model for predicting chemical carcinogenicity and underlying mode of action. Exp Toxicol Pathol 2014;66:313–21.

Mei N, Arlt VM, Phillips DH, Heflich RH, Chen T. DNA adduct formation and mutation induction by aristolochic acid in rat kidney and liver. Mutat Res 2006;602:83–91.

Mengs U, Lang W, Poch JA. The carcinogenic action of aristolochic acid in rats. Arch Toxicol 1982;51:107–19.

Mizerovská J, Dračínská H, Frei E, Schmeiser HH, Arlt VM, Stiborová M. Induction of biotransformation enzymes by the carcinogenic air-pollutant 3-nitrobenzanthrone in liver, kidney and lung, after intra-tracheal instillation in rats. Mutat Res 2011;720:34–41.

Müller D, Strasser FF. Comparative studies on the Chinese hamster bone marrow after treatment with phenylbutazone and cyclophosphamide. Mutat Res 1971;13:377–82.

Mulroney SE, Koenig JI, Csikos T, Pesce C, Striker L, LeRoith D, et al. Temporal changes in insulin-like growth factor I, c-fos, and c-jun gene expression during hyperplastic kidney growth in weanling rats. Endocrinology 1996;137:839–45.

Mulroney SE, Pesce C. Early hyperplastic renal growth after uninephrectomy in adult female rats. Endocrinology 2000;141:932–7.

National Toxicology Program. Chemicals associated with site-specific neoplasia; 2014, Available from URL (http://ntp.niehs.nih.gov/results/summaries/organs/sa-pos.html) (Cited 1 August 2014).

National Toxicology Program. Toxicology and carcinogenesis studies of d-limonene (CAS No. 5989-27-5) in F344/N rats and B6C3F1 mice (gavage studies). Natl Toxicol Program Tech Rep Ser 1990a;347:1–165.

National Toxicology Program. Toxicology and carcinogenesis studies of phenylbutazone (CAS no. 50-33-9) in F344/N rats and B6C3F1 mice (gavage studies). Natl Toxicol Program Tech Rep Ser 1990b;367:1–205.

Nogueira E. Rat renal carcinogenesis after chronic simultaneous exposure to lead acetate and *N*-nitrosodiethylamine. Virchows Arch B Cell Pathol Incl Mol Pathol 1987;53:365–74.

Nohmi T, Suzuki T, Masumura K. Recent advances in the protocols of transgenic mouse mutation assays. Mutat Res 2000;455:191–215.

Priestap HA, Torres MC, Rieger RA, Dickman KG, Freshwater T, Taft DR, et al. Aristolochic acid I metabolism in the isolated perfused rat kidney. Chem Res Toxicol 2012;25:130–9.

Radford R, Frain H, Ryan MP, Slattery C, McMorrow T. Mechanisms of chemical carcinogenesis in the kidneys. Int J Mol Sci 2013;14:19416–33.

Rathenberg R, Müller D. Comparative cytogenetic studies of the influence of phenylbutazone and cyclophosphamide on spermatogenesis in the mouse. Agents Actions 1972;2:180–5.

Rutenburg AM, Kim H, Fischbein JW, Hanker JS, Wasserkrug HL, Seligman AM. Histochemical and ultrastructural demonstration of gamma-glutamyl transpeptidase activity. J Histochem Cytochem 1969;17:517–26.

Tasaki M, Kuroiwa Y, Inoue T, Hibi D, Matsushita K, Ishii Y, et al. Oxidative DNA damage and *in vivo* mutagenicity caused by reactive oxygen species generated

in the livers of p53-proficient or -deficient *gpt* delta mice treated with non-genotoxic hepatocarcinogens. J Appl Toxicol 2013;33:1433–41.

Tsuda H, Futakuchi M, Fukamachi K, Shirai T, Imaida K, Fukushima S, et al. Medium-term, rapid rat bioassay model for the detection of carcinogenic potential of chemicals. Toxicol Pathol 2010;38:182–7.

Tsuda H, Lee G, Farber E. Induction of resistant hepatocytes as a new principle for a possible short-term *in vivo* test for carcinogens. Cancer Res 1980;40:1157–64.

Umemura T, Kitamura Y, Kanki K, Maruyama S, Okazaki K, Imazawa T, et al. Dose-related changes of oxidative stress and cell proliferation in kidneys of male and female F344 rats exposed to potassium bromate. Cancer Sci 2004;95: 393–8.

Umemura T, Kodama Y, Kurokawa Y, Williams GM. Lack of oxidative DNA damage or initiation of carcinogenesis in the kidneys of male F344 rats given subchronic exposure to *p*-dichlorobenzene (pDCB) at a carcinogenic dose. Arch Toxicol 2000;74:54–9.

Umemura T, Tasaki M, Kijima A, Okamura T, Inoue T, Ishii Y, et al. Possible participation of oxidative stress in causation of cell proliferation and *in vivo* mutagenicity in kidneys of *gpt* delta rats treated with potassium bromate. Toxicology 2009;257:46–52.

Xing G, Qi X, Chen M, Wu Y, Yao J, Gong L, et al. Comparison of the mutagenicity of aristolochic acid I and aristolochic acid II in the gpt delta transgenic mouse kidney. Mutat Res 2012;743:52–8.

1521-009X/43/11/1815–1822$25.00
DRUG METABOLISM AND DISPOSITION

http://dx.doi.org/10.1124/dmd.115.065060
Drug Metab Dispos 43:1815–1822, November 2015

New Photosafety Assessment Strategy Based on the Photochemical and Pharmacokinetic Properties of Both Parent Chemicals and Metabolites

Masashi Kato, Gen Suzuki, Hiroto Ohtake, Yoshiki Seto, and Satomi Onoue

Department of Pharmacokinetics and Pharmacodynamics, School of Pharmaceutical Sciences, University of Shizuoka, Suruga-ku, Shizuoka, Japan

Received April 29, 2015; accepted August 19, 2015

ABSTRACT

Photoreactivity and dermal/ocular deposition of compounds have been recognized as key considerations for evaluating the phototoxic risk of compounds. Because some drugs are known to cause phototoxic reactions via generation of potent phototoxic metabolites, photosafety assessments on parent drugs alone may lead to false predictions about their photosafety. This study aimed to establish a new photosafety assessment strategy for evaluating the in vivo phototoxic potential of both a parent substance and its metabolites. The in vivo phototoxic risk of fenofibrate (FF) and its metabolites, fenofibric acid (FA) and reduced fenofibric acid, were evaluated based on photochemical and pharmacokinetic analyses. FF and FA exhibited intensive UV absorption, with molar extinction coefficient values of 17,000 (290 nm) and 14,000 $M^{-1}cm^{-1}$ (295 nm), respectively. Superoxide generation from FA was significantly higher than from FF, and a marked increase in superoxide generation from FF was observed after incubation with rat hepatic S9 fractions, suggesting enhanced photoreactivity of FF after metabolism. FA showed high dermal/ocular deposition after oral administration (5 mg/kg, p.o.) although the concentration of FF was negligible, suggesting high exposure risk from FA. On the basis of these findings, FA was deduced to be a major contributor to phototoxicity induced by FF taken orally, and this prediction was in accordance with the results from in vitro/in vivo phototoxicity tests. Results from this study suggest that this new screening strategy for parent substances and their metabolites provides reliable photosafety information on drug candidates and would be useful for drug development with wide safety margins.

Introduction

Drug-induced photosensitivity can be elicited by topical or systemic application of pharmaceutical substances in combination with subsequent exposure to sunlight or artificial light (Moore, 2002; Drucker and Rosen, 2011). Because the photochemical reactions of drug molecules are a key trigger of phototoxic reactions, photochemical evaluations such as UV spectral analysis and reactive oxygen species (ROS) assays are carried out as photosafety assessments in pharmaceutical research to avoid adverse phototoxic events (Onoue et al., 2009; Seto et al., 2012). In addition to photochemical evaluation, pharmacokinetic (PK) evaluation with a focus on sunlight-exposed tissues (e.g., skin and eyes) can also be helpful for predicting in vivo phototoxicity, because phototoxic reactions mainly occur in the skin (Seto et al., 2009, 2011). Currently, regulatory agencies recommend PK characterization as well as photochemical characterization for photosafety assessment of pharmaceuticals. For example, tissue distribution is recommended in the guidelines for photosafety assessment of pharmaceuticals published by the International Conference on Harmonisation of Technical Requirements for Registration of Pharmaceuticals for Human Use (ICH) in 2014.

In many cases of drug-induced photosensitivity, phototoxic reactions are thought of as mainly being elicited by parent drugs, and the photosafety of drug metabolites is, in principle, outside the scope of regulatory oversight (according to the 2014 ICH S10 guideline). However, the metabolites of phototoxic compounds can have phototoxicity that is as potent as that of their parent drugs, and some metabolites have even more potent phototoxic potential than their parent chemicals, including amiodarone, chlorpromazine, and fenofibrate (FF) (Ljunggren, 1977; Ljunggren and Möller, 1977; Ferguson et al., 1985; Miranda et al., 1994). In our previous investigation, in vivo phototoxic risk of chlorpromazine was predicted to be less phototoxic on the basis of the photochemical and PK characteristics of its parent compounds, although a potent in vivo phototoxic reaction was in fact observed in the rat skin after oral administration of chlorpromazine (Onoue et al., 2014a). Previous studies have shown that chlorpromazine taken orally is extensively metabolized by cytochrome P450 (Wójcikowski et al., 2010), and its demethylated metabolites are more phototoxic than chlorpromazine (Ljunggren and Möller, 1977). In this context, false predictions might

This research was supported in part by the Ministry of Health, Labour and Welfare of Japan [Health Labour Sciences Research Grant H25-iyaku-wakate-024], the Cosmetology Research Foundation [Grant 527], and the Hoyu Science Foundation [Grant 31].
dx.doi.org/10.1124/dmd.115.065060.

ABBREVIATIONS: 3T3 NRU PT, 3T3 neutral red uptake phototoxicity test; $AUC_{0-\infty}$, area under the concentration versus time curve from time 0 to ∞ after administration; DMSO, dimethylsulfoxide; FA, fenofibric acid; FF, fenofibrate; ICH, International Conference on Harmonisation of Technical Requirements for Registration of Pharmaceuticals for Human Use; MEC, molar extinction coefficient; MPE, mean photo effect; mROS, micellar reactive oxygen species; NBT, nitroblue tetrazoleum; PK, pharmacokinetic; QN, quinine; RFA, reduced fenofibric acid; ROS, reactive oxygen species; SB, sulisobenzone; UPLC/ESI-MS, ultra-performance liquid chromatography equipped with electrospray ionization mass spectrometry.

arise from the lack of photochemical and PK characterization of metabolites, and the photosafety assessments of metabolites as well as their parent chemicals should provide more reliable photosafety information on pharmaceuticals; however, the feasibility of such new screening strategies is unknown.

This study aimed to establish a new photosafety assessment strategy with the combined use of photochemical and PK characterization on a parent drug and its metabolites, applying this new screening strategy to FF and its major metabolites, fenofibric acid (FA) and reduced fenofibric acid (RFA) (Fig. 1). FF, an antihyperlipoproteinemic agent, is clinically recognized as phototoxic (Roberts, 1989; Leenutaphong and Manuskiatti, 1996; Machet et al., 1997), and the phototoxic potential of FF has been investigated using several in vitro tools, demonstrating the potent in vitro phototoxicity of FF and FA (Vargas et al., 1993; Miranda et al., 1994). Thus, in this study, FF and its metabolites were employed as model chemicals to confirm the feasibility of the new screening strategy. The photoreactivity of these compounds was evaluated by UV spectral analyses and ROS determination before and after incubation with rat hepatic/intestinal S9 fractions. Dermal and ocular deposition of FF and its metabolites was characterized after the oral administration of FF to rats.

Materials and Methods

Chemicals. FF was purchased from Wako Pure Chemical Industries (Osaka, Japan). FA and RFA were bought from AK Scientific Inc. (Union City, CA) and Toronto Research Chemicals Inc. (Toronto, Ontario, Canada), respectively. Pooled IGS Sprague-Dawley rat liver S9 fractions, pooled IGS Sprague-Dawley rat intestinal S9 fractions, and an NADPH-regenerating system were obtained from Sekisui Medical (Tokyo, Japan). All other reagents were purchased from commercial sources. A quartz reaction container for irradiation of simulated sunlight to a 96-well plate was constructed by Ozawa Science (Aichi, Japan).

UV Spectral Analysis. UV spectral analysis was performed as previously described (Seto et al., 2013b) with minor modifications. Briefly, FF (20 μM) was not dissolved in 20 mM sodium phosphate buffer (NaPB, pH 7.4) due to its poor solubility; thus, each compound was dissolved in ethanol at a final concentration of 20 μM. UV absorption spectra were recorded with a Hitachi U-2010 spectrophotometer (Hitachi High-Technologies Corporation, Tokyo, Japan) interfaced to a PC for data processing (Spectra Manager software; JASCO, Easton, MD). A spectrofluorometer quartz cell with a 10-mm pathlength was employed. Molar extinction coefficient (MEC) values were calculated on the basis of maximum absorbance values in the wavelength range of 290–400 nm.

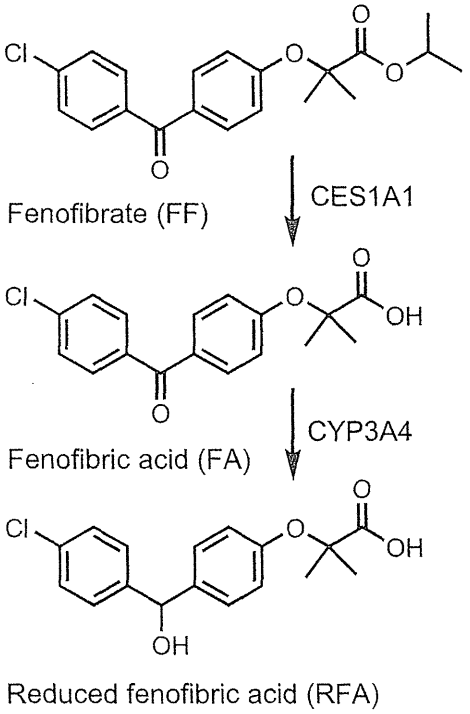

Fig. 1. Major metabolic pathways of FF in rats, monkeys, and humans. FF is metabolically transformed into FA and RFA (Miller and Spence, 1998; Fukami et al., 2010).

Irradiation Conditions for Determination of ROS. An Atlas Suntest CPS+ (Atlas Material Technology LLC, Chicago, IL) equipped with a 1500 W xenon arc lamp and a SR-P20FLE cooling unit (Hitachi, Tokyo, Japan) was used to determine ROS from irradiated chemicals. A UV special filter was installed to adapt the spectrum of the artificial light source to that of natural daylight; the Atlas Suntest CPS series has a high irradiance capability that meets International Commission on Illumination CIE85/1989 daylight simulation requirements. The irradiation test was carried out at 25°C with an irradiance of approximately 2.0 mW/cm^2 as determined with a calibrated Dr. Hönle 0037 UVA detector (Munich, Germany).

Determination of ROS from Photoirradiated Compounds. Determination of singlet oxygen and superoxide generated from photoirradiated compounds was conducted in accordance with an established protocol (Seto et al., 2013a). Briefly, each tested compound was dissolved in dimethylsulfoxide (DMSO) at 10 mM as a stock solution. To monitor the generation of singlet oxygen, samples containing compounds (200 μM), *p*-nitrosodimethylaniline (50 μM), and imidazole (50 μM) in 20 mM NaPB (pH 7.4) with 0.5% (v/v) Tween 20 were irradiated with simulated sunlight, and then the UV absorption at 440 nm was measured using the Safire plate reader (TECAN, Männedorf, Switzerland). To determine superoxide generation, samples containing the compounds (200 μM) and nitroblue tetrazolium (NBT; 50 μM) in 20 mM NaPB (pH7.4) with 0.5% (v/v) Tween 20 were exposed to simulated sunlight, and the reduction of NBT was measured by the increase in the absorbance at 560 nm using the Safire plate reader. According to the results (mean of triplicate determinations) from the micellar reactive oxygen species (mROS) assay, photoreactivity for each tested chemical should be judged to be 1) positive with singlet oxygen ($\Delta A_{440\ nm} \times 10^3$): 25 or more, and/or superoxide ($\Delta A_{560\ nm} \times 10^3$): 20 or more; or 2) negative with singlet oxygen ($\Delta A_{440\ nm} \times 10^3$): less than 25, and superoxide ($\Delta A_{560\ nm} \times 10^3$): less than 20. In the mROS assay, the final decision should be made as follows: 1) positive: above the threshold level for singlet oxygen or superoxide; or 2) negative: below the threshold level for both singlet oxygen and superoxide (Onoue et al., 2013a).

Determination of ROS from Photoirradiated Compounds in Enzyme-Treated Samples. Rat hepatic/intestinal S9 fractions were preincubated for 2 minutes at 37°C (final concentration: 0.2 mg protein/ml) in 0.3 ml phosphate buffer (pH 7.4) containing typical cofactors. FF was dissolved in DMSO at 10 mM as a stock solution. The reaction was initiated by the addition of FF at 100 μM, and the final concentration of DMSO was 1%. The reaction was terminated at 1 minute by adding 0.2 ml ice-cold ethanol. For comparison, FF (100 μM) was also incubated with heat-inactivated (approximately 80°C, 5 minutes) S9 fractions (denatured groups). The mixtures were evaluated by a ROS assay (Onoue et al., 2013a). Briefly, to monitor the generation of singlet oxygen, enzyme-treated mixtures, *p*-nitrosodimethylaniline (50 μM), and imidazole (50 μM) was dissolved in 20 mM NaPB (pH 7.4). To determine superoxide generation, the enzyme-treated mixtures and NBT (50 μM) were dissolved in 20 mM NaPB (pH 7.4). Both reaction mixtures theoretically contained 50 μM FF. These samples were then irradiated with simulated sunlight and measured in the same conditions as with the ROS assay protocol.

Animals. Male Sprague-Dawley rats aged 11 to 12 weeks (approximately 300–350 g body weight) were purchased from SLC Inc. (Hamamatsu, Japan). For PK experiments, rats (n = 39) were fasted for approximately 18 hours before drug administration and orally received an ethanolic solution of FF at a dose of 5 mg/kg. For in vivo phototoxicity testing, rats (n = 16) were anesthetized using pentobarbital (50 mg/kg i.p.), and then the hair on the abdomen was shaved at approximately 18 hours before dermal application of the drug solution. All of the procedures used in this study were conducted according to the guidelines approved by the Institutional Animal Care and Ethical Committee of University of Shizuoka.

PK Studies. Blood samples were taken in a volume of 200 μl from the tail vein at the indicated periods (0.5, 1, 2, 3, 4, 6, 8, 12, 24, and 48 hours) after drug administration. The blood samples were centrifuged (10,000 × g, 10 minutes, 4°C) to prepare plasma

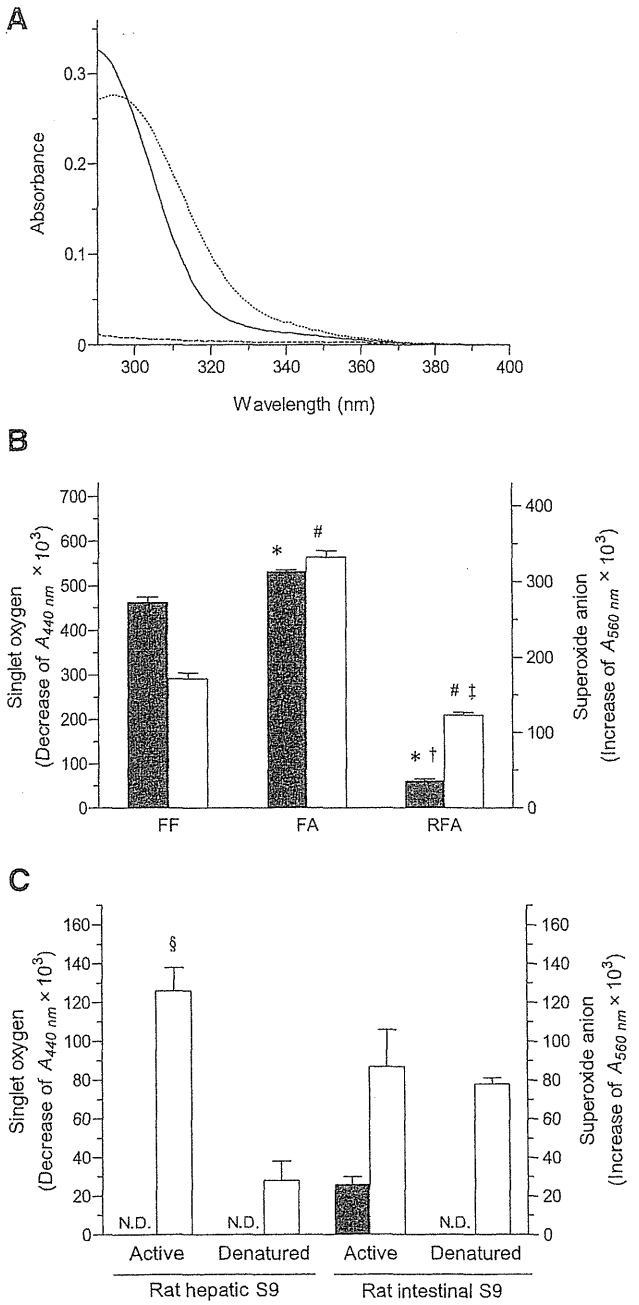

Fig. 2. Photochemical properties of FF and metabolites. (A) UV absorption spectra of compounds (20 μM) in ethanol. Solid line, FF; dashed line, RFA; dotted line, FA. (B) Generation of ROS from each test compound (200 μM). Filled bars, generation of singlet oxygen; open bars, generation of superoxide. $^*P < 0.05$ versus FF within singlet oxygen; $^\dagger P < 0.05$ versus FA within singlet oxygen; $^\#P < 0.05$ versus FF within superoxide; $^\ddagger P < 0.05$ versus FA within superoxide. Data represent the mean ± S.D. (n = 3). (C) Generation of ROS from enzyme-treated FF. $^\S P < 0.05$ versus superoxide in denatured rat hepatic S9 fractions. Data represent the mean ± S.D. (n = 3). N.D., not detected.

samples, and then the samples (100 μl) were deproteinized by the addition of acetonitrile (250 μl). The supernatants were obtained by centrifugation (2000 rpm, 1 minute, 4°C) and filtration (0.20-μm membrane filter, Millex-LG; Millipore, Billerica, MA) and were kept frozen at –20°C until they were analyzed.

At the indicated times (2, 4, 6, 8, 10, 12, 24, and 48 hours) after oral administration of FF, rats were humanely euthanized by taking blood from the descending aorta under anesthesia with pentobarbital Na (50 mg/kg), and the tissues were then perfused with cold saline from the aorta. The skin and eye were dissected, minced with scissors, and homogenized using Physcotron (Microtec, Chiba, Japan) in 4 ml acetonitrile. After sonication for 10 minutes and shaking for 10 minutes, the samples were centrifuged (3000 rpm, 10 minutes). Extraction was repeated twice with acetonitrile, and the supernatants were pooled. The collected eluents were pooled with acetonitrile extracts, and the samples were evaporated to dryness under a gentle stream of nitrogen at 45°C. The extracted and evaporated tissue samples were stored at 4°C until they were analyzed.

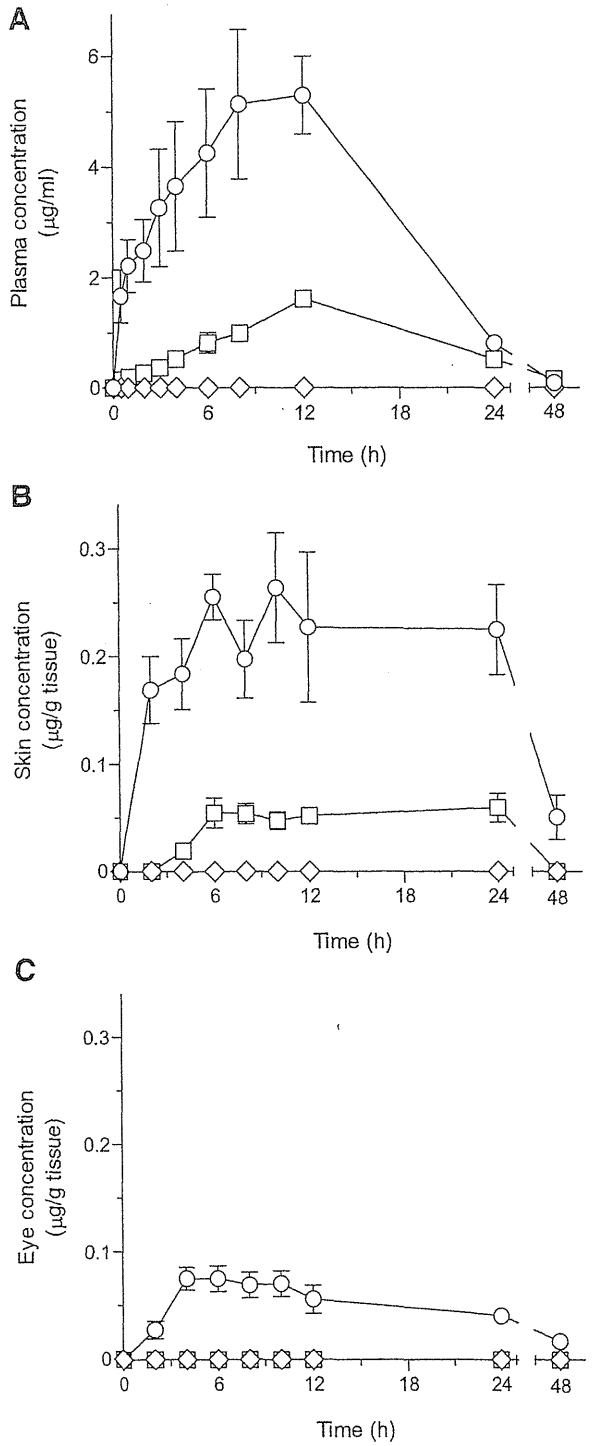

Fig. 3. Concentration-time profiles of FF, FA, and RFA after oral administration of FF (5 mg/kg) in rats. (A–C) Concentrations in plasma (A), skin (B), and eyes (C). Open diamonds, FF; open circles, FA; open squares, RFA. Data represent the mean ± S.E.M. (n = 4–7).

TABLE 1

Pharmacokinetic parameters in plasma, skin, and eyes after oral administration of fenofibrate in rats

Samples	$t_{1/2}$ (*h*)	C_{max} (*μg/ml or μg/g tissue*)	T_{max} (*h*)	$AUC_{0-\infty}$ (*h·μg/ml or h·μg/g tissue*)	MRT (*h*)
FF					
Plasma	N.A.	N.A.	N.A.	N.A.	N.A.
Skin	N.A.	N.A.	N.A.	N.A.	N.A.
Eye	N.A.	N.A.	N.A.	N.A.	N.A.
FA					
Plasma	6.4 ± 0.40	6.3 ± 1.1	9.7 ± 1.1	97 ± 14	13 ± 0.70
Skin	11 ± 1.5	0.34 ± 0.017	13 ± 3.9	8.5 ± 1.3	20 ± 2.1
Eye	22 ± 6.9	0.10 ± 0.0055	6.0 ± 1.4	2.6 ± 0.33	34 ± 10
RFA					
Plasma	12 ± 1.0	1.6 ± 0.10	12 ± 0.0	33 ± 3.2	21 ± 1.5
Skin	17 ± 3.3	0.080 ± 0.0067	16 ± 4.7	2.0 ± 0.60	30 ± 4.2
Eye	N.A.	N.A.	N.A.	N.A.	N.A.

$AUC_{0-\infty}$, area under the concentration *vs.* time curve from t=0 to t=∞ after administration; C_{max}, maximum concentration; $t_{1/2}$, terminal half-life; T_{max}, time to maximum concentration; and MRT, mean residence time. Each value represents the mean±SEM for 4–7 rats. N.A., not available due to concentrations below the limit of detection.

To determine drug concentrations in plasma and tissue samples, an ultra-performance liquid chromatography equipped with electrospray ionization mass spectrometry (UPLC/ESI-MS) system was employed (Onoue et al., 2013b). The UPLC-ESI/MS system consisted of a Waters Acquity UPLC system (Waters, Milford, MA), which included a binary solvent manager, a sample manager, a column compartment, and a micromass SQ detector connected with Waters MassLynx (version 4.1). A Waters Acquity UPLC BEH C18 column (particle size, 1.7 μm; and column size, Φ2.1 × 50 mm; Waters) was used, and the column temperature was maintained at 40°C. The deproteinized plasma samples were mixed with 50% acetonitrile solution containing ketoprofen (1 μg/ml), an internal standard for UPLC/ESI-MS analysis (1:1 ratio of supernatant/ketoprofen). To determine tissue concentration, the extracted and evaporated samples were dissolved in 50% acetonitrile including ketoprofen (500 ng/ml). The standards and samples were separated using a gradient mobile phase consisting of purified water containing 0.1% formic acid (A) and acetonitrile (B). The gradient conditions of the mobile phase were as follows: 0 to 1.0 minute, 50% B; 1.0 to 5.0 minutes, 50% to 95% B (linear gradient curve); 5 to 5.5 minutes, 95% B; and 5.5 to 6 minutes, 50% B. The flow rate was set at 0.25 ml/min. Analyses were carried out by monitoring specific mass-to-charge ratios as follows: 361.2 $[M + H]^+$ for FF, 319.2 $[M + H]^+$ for FA, 303 $[M - OH]^+$ for RFA, and 255.2 $[M + H]^+$ for ketoprofen (internal standard).

3T3 Neutral Red Uptake Phototoxicity Testing. Balb/c 3T3 mouse fibroblast cells (CloneA-31) were maintained in culture as previously reported (Spielmann et al., 1991). The 3T3 neutral red uptake phototoxicity test (3T3 NRU PT) and data analyses were carried out as described in the 2004 Organisation for Economic Co-operation and Development Guideline 432. Briefly, Balb/c 3T3 cells were maintained in culture for 24 hours for the formation of monolayers. Two 96-well plates per test chemical were then preincubated with six different concentrations of the chemical dissolved in Earle's balanced salt solution for 1 hour in duplicate. One plate was then exposed to a dose of 5 J/cm^2 UVA (irradiation experiment), whereas the other plate was kept in the dark by covering it with aluminum foil (nonirradiation experiment). UVA irradiation (approximately 30 minutes) was performed using a SOL 500 Sun simulator (Dr. Hönle) equipped with a 500 W metal halide lamp and an H-1 filter to remove potentially cytotoxic UVB wavelengths. The treatment medium was then replaced with culture medium; after 24 hours, cell viability was determined by neutral red uptake for 3 hours. After that, cells were lysed in eluate (50:49:1 ratio of ethanol/water/acetic acid), and neutral red uptake was measured at an absorbance of 540 nm using the Benchmark Plus microplate spectrophotometer (BioRad, Hercules, CA). Cell viability obtained with each of the six concentrations of the test chemical was compared with that of untreated controls, and mean photo effect (MPE) values were calculated by using Phototox software (version 2.0; ZEBET, Berlin, Germany) on the basis of obtained cell viability curves in UVA-irradiated and nonirradiated groups of the test chemical for evaluating in vitro phototoxicity.

In Vivo Phototoxicity Testing. Experiments were performed as described previously, with minor changes in dermal administration (Seto et al., 2009). Each FF, FA, or control [quinine (QN) and sulisobenzone (SB)] was dissolved in DMSO at 100 mg/ml and was applied to two application sites on rat skin at the abdomen (10 mg/site, $n = 4$) using filter paper (2 cm × 2 cm) under anesthesia with pentobarbital Na (50 mg/kg). At 4 hours after dermal administration, the filter papers containing chemicals on the application sites were removed and wiped using cotton soaked with distilled water. Rats were then irradiated individually using black light (FL15BL-B; National, Tokyo, Japan) as a UVA light source with an irradiance of approximately 2.7 mW/cm^2 for approximately 3 hours until the UV irradiance level reached 30 J/cm^2. Because UVB light is highly cytotoxic, a UVA light source was employed for the in vivo phototoxicity testing. During the UVA irradiation, rats were restrained on a sunbed under anesthesia with pentobarbital Na (50 mg/kg) to ensure uniform irradiation of their abdomen, and nonirradiated sites were wrapped in aluminum foil for protection from UV light. UV intensity was monitored using the calibrated Dr. Hönle 0037 UVA detector. A colorimeter equipped with a data processor (NF333; Nippon Denshoku, Tokyo, Japan) was used as a measure of skin color. This instrument records three-dimensional color reflectance, the so-called $L^*a^*b^*$ system, as recommended by the International Commission on Illumination. The luminance (L^*) gives the relative brightness ranging from total black ($L^* = 0$) to total white ($L^* = 100$). The hue (a^*) axis represents the balance between red (positive values up to 100) and green (negative values up to −100), and the chroma (b^*) axis represents the balance between yellow (positive values up to 100) and blue (negative values up to −100). The differences in skin color (ΔE) between before and after irradiation were described as follows (Westerhof et al., 1986; Piérard and Piérard-Franchimont, 1993):

$$\Delta E = \sqrt{(\Delta L^*)^2 + (\Delta a^*)^2 + (\Delta b^*)^2}$$

Data Analysis. The significance of differences was determined by *t* tests on the data from ROS generation after incubation with rat hepatic/intestinal S9 fractions. Other data were analyzed by one-way analysis of variance followed by Tukey's multiple comparison tests. $P < 0.05$ was considered significant for all analyses. PK characterizations were performed by noncompartmental analysis as implemented in WinNonlin Professional software (version 5.2; Pharsight Corporation, Mountain View, CA).

Results

Photochemical Characterization. Phototoxic reactions can be triggered by photochemical reactions of drug molecules after absorption of UV and visible light (290–700 nm) (Moore, 1998; Onoue and Tsuda, 2006). Herein, the photochemical properties of FF and two major metabolites, FA and RFA, were analyzed with a focus on UV-absorbing properties and ROS-generating potentials. FF and FA exhibited intensive UVA/UVB absorption, with maximal MEC values of 17,000 (290 nm) and 14,000 $M^{-1}cm^{-1}$ (295 nm); by contrast, only weak

UVB absorption was observed in RFA, with an MEC of 850 $M^{-1}cm^{-1}$ at 290 nm (Fig. 2A). Drug molecules with an MEC of less than 1000 $M^{-1}cm^{-1}$ were previously demonstrated to be less phototoxic (Henry et al., 2009); thus, FF and FA can be identified as photoexcitable.

To clarify the photoreactivity of FF and its metabolites, the generation of ROS from these compounds (200 μM) was determined under irradiation of simulated sunlight (Fig. 2B) since the good relationship between ROS data on chemicals at 200 μM and in vivo phototoxicity revealed the prediction capacity of the ROS assay (Onoue and Tsuda, 2006; Onoue et al., 2008a). FF and FA exhibited potent generation of singlet oxygen, with values of 463 and 531 ($\Delta A_{440\ nm} \times 10^3$), respectively; they also generated superoxide, with values of 171 and 332 ($\Delta A_{560\ nm} \times 10^3$). The levels of ROS generation from RFA were lower than those from FF and FA, and the values of singlet oxygen and superoxide generation were 61 ($\Delta A_{440\ nm} \times 10^3$) and 123 ($\Delta A_{560\ nm} \times 10^3$), respectively. From these findings, all compounds were judged to be photoreactive according to the ROS data–based classification system, and the photoreactivity of the compounds was ranked as follows: FA > FF ≫ RFA.

ROS generation from enzyme-treated FF was determined after incubation with rat hepatic/intestinal S9 fractions to evaluate the possible photochemical transitions of FF after metabolism (Fig. 2C). Although no significant differences were observed in ROS generation from FF between pretreatment of active and denatured rat intestinal S9 fractions, the generation of superoxide from FF was significantly increased by approximately 4.5-fold after preincubation with active rat hepatic S9 fractions compared with that from FF incubated with the denatured one ($P < 0.05$), suggesting enhanced photoreactivity of FF after metabolism in the liver.

PK Characterization. Phototoxic reactions mainly occur in the skin and eyes; thus, dermal and ocular exposure to compounds can be a predictive factor for in vivo phototoxicity as well as systemic exposure (Boiy et al., 2008; Seto et al., 2009). PK characterizations of compounds were conducted with a focus on plasma, skin, and eyes (Fig. 3; Table 1). After oral administration of FF to rats, FF was negligible in all tissues (below the limit of detection: 10 ng/ml and 7.1 ng/g tissue), whereas its metabolites could be detected in plasma and tissues. A rapid and sustained increase in the FA level was observed in all tissues up to 6.0–13 hours, whereas RFA concentrations in the plasma and skin were gradually elevated (T_{max} of 12–16 hours). The C_{max} and area under the concentration versus time curve from time 0 to ∞ after administration ($AUC_{0-\infty}$) values in plasma and skin of FA were approximately 3- to 4-fold higher than those of RFA, and only FA could be detected in rat eyes, with C_{max} and $AUC_{0-\infty}$ values of 0.10 μg/g tissue and 2.6 h · μg/g tissue, respectively. Therefore, FA would have a higher exposure risk of UV-exposed tissues compared with RFA. By contrast, RFA exhibited slower elimination from the plasma and skin compared with FA, as evidenced by the approximately 1.5- to 2-fold–longer apparent half-lives of RFA compared with FA in the plasma and skin, suggesting longer tissue retention of RFA. From the PK characteristics, dermal and ocular exposure was ranked as follows: FA > RFA ≫ FF.

Comparative In Vitro/In Vivo Photosafety Assessments. When both photochemical and PK data are taken into account, FA was more likely to be phototoxic than the others; the photosafety of FA was then examined by both 3T3 NRU PT, a well validated alternative method for photosafety assessment (Spielmann et al., 1998), and the rat in vivo phototoxicity test. FF was also tested for comparison. QN and SB were employed as positive/negative controls in both in vitro/in vivo photosafety tests, respectively. In 3T3 NRU PT, cell viability curves were almost identical between UV-irradiated and nonirradiated groups treated with SB (Fig. 4A). By contrast, QN induced potent phototoxicity

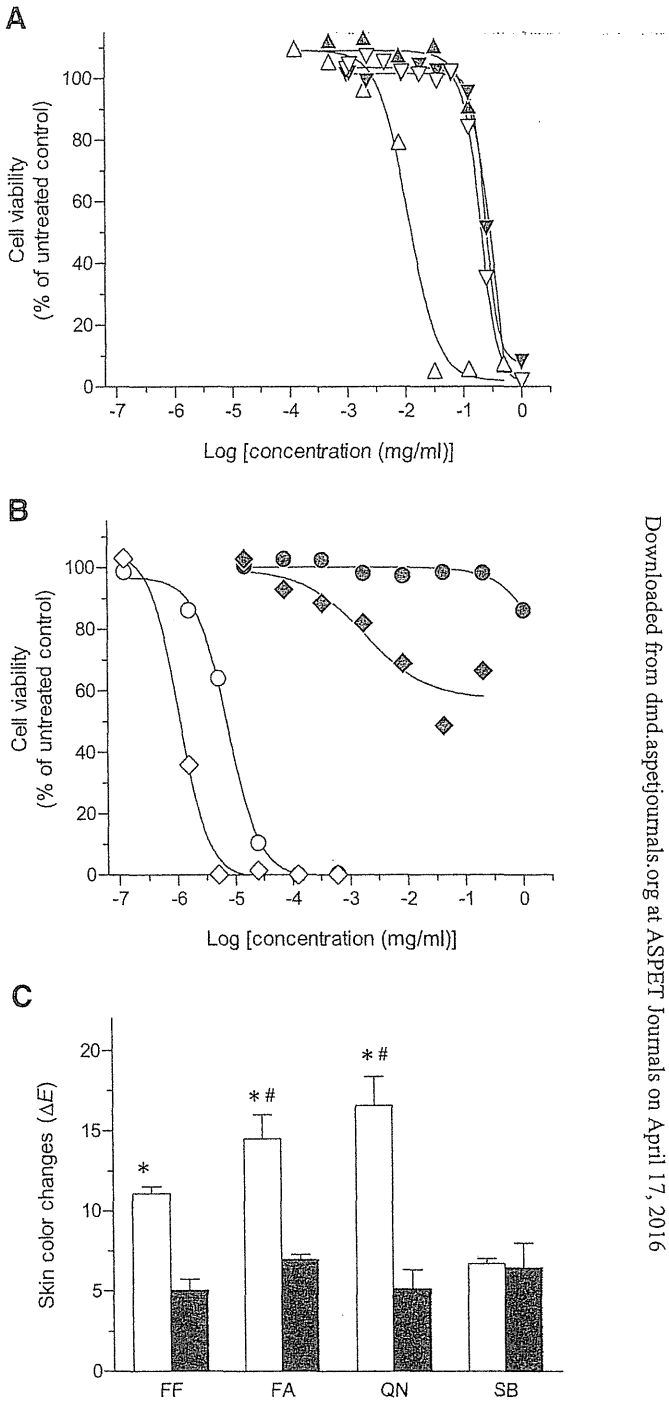

Fig. 4. In vitro/in vivo phototoxicity tests on QN, SB, FF, and FA. (A and B) 3T3 NRU phototoxicity testing on positive/negative controls (A) and FF and FA (B). Upward triangles, QN; downward triangles, SB; diamonds, FF; circles, FA. Open symbols, UV-irradiated groups; filled symbols, nonirradiated groups. Data represent the mean of duplicate measurements. (C) Colorimetric evaluation (ΔE) of phototoxic skin responses in rats. Open bars, UV-irradiated groups; filled bars, nonirradiated groups. $^*P < 0.05$ versus the nonirradiated group of each compound; $^{\#}P < 0.05$ versus SB within UV-irradiated groups. Data represent the mean ± S.E.M. ($n = 4$).

to 3T3 cells after UV irradiation. As observed for QN, FF and FA also exhibited enhanced cell death upon UV exposure, indicating potent phototoxicity to 3T3 cells (Fig. 4B). MPE values can distinguish phototoxic molecules (MPE ≥ 0.1) from nonphototoxic ones (MPE < 0.1) (Holzhutter, 1997), and MPE values of FF and FA were 0.40 and

0.54, respectively. Therefore, both FF and FA were identified as phototoxic, and FA would be more phototoxic to 3T3 cells than FF because of its larger MPE value.

In vivo photosafety profiles were assessed based on the transitions in skin color (ΔE) after UV irradiation after dermal administration of FF, FA, QN, and SB (Fig. 4C). Dermal concentrations of FF and FA did not increase from 2 to 6 hours after dermal application (data not shown), suggesting steady-state concentrations of the drugs in the skin; then, the application period was confirmed at 4 hours in this study. In SB-treated groups, no significant differences were observed between UV-irradiated and nonirradiated rats. On the other hand, upon UV irradiation, QN induced a significant increase in the ΔE value owing to the increase in the Δb^* value, as previously observed (Nose and Tsurumi, 1993). UV-irradiated FF and FA also exhibited significantly higher ΔE values than each nonirradiated group ($P < 0.05$), and these color changes were due to significant increases of Δb^* values by 6.4 (for FF) and 5.9 (for FA). Furthermore, in FA-treated groups, the Δa^* value was also significantly increased by 4.7 upon UV irradiation. Although ΔE values were not significantly different between UV-irradiated FF and UV-irradiated SB, the ΔE value of UV-exposed rats treated with FA was significantly higher than that of UV-exposed rats treated with SB ($P < 0.05$). These results demonstrated more severe phototoxicity of FA than FF to rat skin.

Discussion

To evaluate in vivo phototoxic risk of a chemical and its metabolites, development of a new photosafety screening system was attempted by photochemical and PK characterization, and the new screening strategy was applied to predict in vivo phototoxic risk of FF and its major metabolites, FA and RFA. According to our outcomes, FA, a major metabolite of FF, can be the major contributor to FF-induced phototoxic skin responses because of its potent photoreactivity and high dermal/ocular exposure.

The primary trigger for phototoxic reactions can be photoexcitation of chemical molecules with UV/visible light irradiation (Moore, 1998); and excited molecules then tend to undergo type I and/or II photochemical reactions with molecular oxygen and/or biomolecules. Generation of superoxide and singlet oxygen from photoirradiated chemicals can be reliable indicators of type I and II photochemical reactivity, respectively (Onoue and Tsuda, 2006; Onoue et al., 2008a). From the ROS data, type I reactivity of FA was higher than that of FF; on the other hand, photoreactivity of RFA would be low among tested chemicals. In addition, enhanced superoxide generation could be observed after preincubation of FF with active rat hepatic S9 fractions compared with the denatured group. Benzophenones including FF and FA can elicit lipid peroxidation, a major mechanism of photoirritation, via type I photochemical reactions after photoexcitation (Marković et al., 1990). In this context, FA might be a major contributor to FF-induced phototoxicity after metabolism of FF. For photosafety assessments, exposure of compounds and their retention to dermal/ocular tissues can also be a key consideration because phototoxic reactions typically occur in the skin and eyes (Boiy et al., 2008; Seto et al., 2009). Therefore, in this study, the PK behavior of FF and its metabolites was assessed with a focus on plasma and skin/eyes in rats after oral administration of FF. Interestingly, FF was negligible in all samples, and only two metabolites could be detected in our PK study. According to our results, FA would have the highest dermal/ocular exposure risk, suggesting a major contribution of FF-induced phototoxicity. Although dermal exposure risk of RFA was lower than FA, RFA might have longer-term dermal exposure risk compared with FA on the basis of its long elimination half-life. For comparison, in vitro/in vivo phototoxicity tests were also conducted, and potent phototoxicity of FF and FA was confirmed. According to the cell viability curves and ΔE values in UV-irradiated groups, the metabolic activity for conversion of FF to FA might not be high in 3T3 cells and rat skin; phototoxicity of FA would be more potent than that of FF on the basis of the data obtained.

In photosafety assessment, both photochemical and PK properties should be taken into consideration; thus, a summary table was built using photochemical and PK data (Table 2), and values among the data are classified as high, moderate, and low levels in accordance with our previous research (Seto et al., 2011). In our photosafety prediction, high levels for both photochemical and PK data might indicate high phototoxic potential, whereas low levels in either or both might be indicative of moderate or low phototoxic potential. FA was deduced to be a highly phototoxic metabolite because both photoreactivity and dermal/ocular exposure were high. FF and RFA were less phototoxic, owing to limited dermal/ocular exposure of FF, moderate photoreactivity, and limited ocular exposure of RFA. In this context, the phototoxic risk of test compounds was deduced as follows: FA $\gg$ RFA $>$ FF (in the skin) and FA $\gg$ RFA = FF (in the eyes). The deduced phototoxic potential of FF and FA was in

TABLE 2

Decision matrix for evaluating in vivo phototoxicity risk of FF and its metabolites

Assays	FF		FA		RFA	
	Value	Level of Intensity	Value	Level of Intensity	Value	Level of Intensity
Photochemical properties						
UV absorbance						
λ_{max} (nm) [ε ($M^{-1}cm^{-1}$)]	290 [17,000]	High	295 [14,000]	High	290 [850]	Low
ROS data						
$^1O_2$ ($\Delta A_{440\ nm} \times 10^3$)	463	High	531	High	61	Low
O_2^- ($\Delta A_{560\ nm} \times 10^3$)	171	Moderate	332	High	123	Moderate
Distribution to UV-exposed tissues						
Skin						
$t_{1/2}$ (h)	N.A.		11	Moderate	17	High
C_{max} (μg/g tissue)	N.A.		0.34	High	0.080	Low
$AUC_{0-\infty}$ (h·μg/g tissue)	N.A.		8.5	High	2.0	Moderate
Eyes						
$t_{1/2}$ (h)	N.A.		22	High	N.A.	
C_{max} (μg/g tissue)	N.A.		0.10	Moderate	N.A.	
$AUC_{0-\infty}$ (h·μg/g tissue)	N.A.		2.6	Moderate	N.A.	

Each crucial factor was divided into three levels of intensity, which are indicated as low, medium, and high. N.A., not available due to concentrations below the limit of detection.

agreement with the phototoxic outcomes from in vitro/in vivo photosafety tests, suggesting the reliability of our photosafety prediction on FF and FA. From these findings, phototoxic events related to FF would be attributed to FA, which might be the reason for the discrepancy between the observed phototoxicity after oral administration and the negative results in the photopatch test of FF (Leenutaphong and Manuskiatti, 1996).

Many drugs seemed to exhibit different PK behavior between humans and nonhuman primates, which may partly be due to species differences of metabolic enzymes such as cytochrome P450 enzymes, esterases, and glucuronidases (Baillie and Rettie, 2011). FF is metabolized into FA by carboxylesterase CES1A1 in the liver after absorption, and a portion of it undergoes carbonyl reduction by CYP3A4 to produce RFA, and these metabolites and their glucuronides are then excreted (Weil et al., 1988, 1990; Cornu-Chagnon et al., 1995; Miller and Spence, 1998; Fukami et al., 2010). Thus, outcomes from PK assessment could not be completely extrapolated to humans as long as interspecies differences existed in the enzymes related to FF metabolism. According to a previous report, no significant differences were reported between human and rat hepatic CES1A1 activity; furthermore, plasma PK behavior of FA in humans was in agreement with PK data in rats obtained in our study (Lovin et al., 2003; Taketani et al., 2007). Thus, FA might also exhibit high dermal exposure in humans as observed in rats. On the other hand, in humans, there appeared to be interindividual variability in PK, efficacy, and safety profiles of orally administered FF owing to the effect of food intake (Davidson et al., 2005). Yun et al. (2006) demonstrated that the oral administration of FF with a high-fat meal can cause significant increases in C_{max} and $AUC_{0-\infty}$ of FA compared with those under fasted conditions in humans; hence, the effect of food intake, especially high-fat meals, might have a major effect on the photosafety of oral FF therapy since dermal exposure of FA might be increased when FF is orally taken with high-fat meals.

To avoid undesired phototoxic events, early identification of a hazard for metabolite-mediated phototoxicity would be of great help in drug discovery. In general, to evaluate a hazard for metabolite-related toxicity without identification of metabolites, several methods have been developed based on a combination strategy of general toxicity tests and in vitro metabolism studies (Ames et al., 1973; Geissler and Faustman, 1988). As for phototoxicity, the phototoxic hazard of metabolites might be evaluated based on transitions of ROS generation from light-irradiated compounds after treatment with metabolizing enzymes, as observed in our study. However, singlet oxygen generation from some irradiated samples was negligible in the ROS assay with S9 fractions, whereas potent singlet oxygen generation from irradiated FF and FA was observed in the mROS assay. Changes in photochemical reactions in the ROS assay were attributed to assay conditions, including the concentration of chemicals and additives (Onoue et al., 2008b, 2013a, 2014b). Although further optimization of assay conditions is needed, the ROS assay employing drug-metabolizing enzymes might become a useful method for hazard identification of metabolite-mediated phototoxicity.

In conclusion, the established photosafety screening on FF with major metabolites could provide reliable photosafety information on FF. The current ICH S10 guideline for photosafety evaluation recommends conducting photochemical testing, in vitro phototoxicity assays, PK studies, and dedicated clinical studies. To avoid false prediction of drug photosafety in humans, these proposed assessments should be applied to both parent substances and their major metabolites in pharmaceutical research and development, possibly resulting in successful development of pharmaceutical products with wide safety margins.

Acknowledgments

The authors thank Philip Hawke (University of Shizuoka Scientific English Program) for critical reading of and editorial assistance with this manuscript.

Authorship Contributions

Participated in research design: Kato, Suzuki, Ohtake, Onoue.
Conducted experiments: Kato, Suzuki, Ohtake.
Contributed new reagents or analytic tools: Kato, Seto, Onoue.
Performed data analysis: Kato, Onoue.
Wrote or contributed to the writing of the manuscript: Kato, Seto, Onoue.

References

Ames BN, Durston WE, Yamasaki E, and Lee FD (1973) Carcinogens are mutagens: a simple test system combining liver homogenates for activation and bacteria for detection. *Proc Natl Acad Sci USA* **70**:2281–2285.
Baillie TA and Rettie AE (2011) Role of biotransformation in drug-induced toxicity: influence of intra- and inter-species differences in drug metabolism. *Drug Metab Pharmacokinet* **26**:15–29.
Boiy A, Roelandts R, van den Oord J, and de Witte PA (2008) Photosensitizing activity of hypericin and hypericin acetate after topical application on normal mouse skin. *Br J Dermatol* **158**:360–369.
Cornu-Chagnon MC, Dupont H, and Edgar A (1995) Fenofibrate: metabolism and species differences for peroxisome proliferation in cultured hepatocytes. *Fundam Appl Toxicol* **26**:63–74.
Davidson MH, Bays H, Rhyne J, Stein E, Rotenberg K, and Doyle R (2005) Efficacy and safety profile of fenofibrate-coated microgranules 130 mg, with and without food, in patients with hypertriglyceridemia and the metabolic syndrome: an 8-week, randomized, double-blind, placebo-controlled study. *Clin Ther* **27**:715–727.
Drucker AM and Rosen CF (2011) Drug-induced photosensitivity: culprit drugs, management and prevention. *Drug Saf* **34**:821–837.
Ferguson J, Addo HA, Jones S, Johnson BE, and Frain-Bell W (1985) A study of cutaneous photosensitivity induced by amiodarone. *Br J Dermatol* **113**:537–549.
Fukami T, Takahashi S, Nakagawa N, Maruichi T, Nakajima M, and Yokoi T (2010) In vitro evaluation of inhibitory effects of antidiabetic and antihyperlipidemic drugs on human carboxylesterase activities. *Drug Metab Dispos* **38**:2173–2178.
Geissler F and Faustman EM (1988) Developmental toxicity of aflatoxin B1 in the rodent embryo in vitro: contribution of exogenous biotransformation systems to toxicity. *Teratology* **37**: 101–111.
Henry B, Foti C, and Alsante K (2009) Can light absorption and photostability data be used to assess the photosafety risks in patients for a new drug molecule? *J Photochem Photobiol B* **96**: 57–62.
Holzhutter HG (1997) A general measure of in vitro phototoxicity derived from pairs of dose-response curves and its use for predicting the in vivo phototoxicity of chemicals. *Altern Lab Anim* **25**:445–462.
International Conference on Harmonization of Technical Requirements for Registration of Pharmaceuticals for Human Use (ICH) (2014) ICH Safety Guideline S10 Photosafety Evaluation of Pharmaceuticals, ICH, Geneva, Switzerland. http://www.ich.org/fileadmin/Public_Web_Site/ICH_Products/Guidelines/Safety/S10/S10_Step_4.pdf
Leenutaphong V and Manuskiatti W (1996) Fenofibrate-induced photosensitivity. *J Am Acad Dermatol* **35**:775–777.
Ljunggren B (1977) Phenothiazine phototoxicity: toxic chlorpromazine photoproducts. *J Invest Dermatol* **69**:383–386.
Ljunggren B and Möller H (1977) Phenothiazine phototoxicity: an experimental study on chlorpromazine and its metabolites. *J Invest Dermatol* **68**:313–317.
Lovin I, Albu F, Tache F, David V, and Medvedovici A (2003) Solvent and salting effects on sample preparation for the determination of fenofibric acid in human plasma by HPLC-DAD. *Microchem J* **75**:179–187.
Machet L, Vaillant L, Jan V, and Lorette G (1997) Fenofibrate-induced photosensitivity: value of photopatch testing. *J Am Acad Dermatol* **37**:808–809.
Marković DZ, Durand T, and Patterson LK (1990) Hydrogen abstraction from lipids by triplet states of derivatized benzophenone photosensitizers. *Photochem Photobiol* **51**:389–394.
Miller DB and Spence JD (1998) Clinical pharmacokinetics of fibric acid derivatives (fibrates). *Clin Pharmacokinet* **34**:155–162.
Miranda MA, Boscá F, Vargas F, and Canudas N (1994) Photosensitization by fenofibrate. II. In vitro phototoxicity of the major metabolites. *Photochem Photobiol* **59**:171–174.
Moore DE (1998) Mechanisms of photosensitization by phototoxic drugs. *Mutat Res* **422**: 165–173.
Moore DE (2002) Drug-induced cutaneous photosensitivity: incidence, mechanism, prevention and management. *Drug Saf* **25**:345–372.
Nose T and Tsurumi K (1993) Pharmacological studies on cutaneous inflammation induced by ultraviolet irradiation (1): quantification of erythema by reflectance colorimetry and correlation with cutaneous blood flow. *Jpn J Pharmacol* **62**:245–256.
Onoue S, Hosoi K, Wakuri S, Iwase Y, Yamamoto T, Matsuoka N, Nakamura K, Toda T, Takagi H, and Osaki N, et al. (2013a) Establishment and intra-/inter-laboratory validation of a standard protocol of reactive oxygen species assay for chemical photosafety evaluation. *J Appl Toxicol* **33**:1241–1250.
Onoue S, Igarashi N, Yamada S, and Tsuda Y (2008a) High-throughput reactive oxygen species (ROS) assay: an enabling technology for screening the phototoxic potential of pharmaceutical substances. *J Pharm Biomed Anal* **46**:187–193.
Onoue S, Kato M, Inoue R, Seto Y, and Yamada S (2014a) Photosafety screening of phenothiazine derivatives with combined use of photochemical and cassette-dosing pharmacokinetic data. *Toxicol Sci* **137**:469–477.
Onoue S, Kato M, and Yamada S (2014b) Development of an albuminous reactive oxygen species assay for photosafety evaluation under experimental biomimetic conditions. *J Appl Toxicol* **34**:158–165.

Onoue S, Seto Y, Gandy G, and Yamada S (2009) Drug-induced phototoxicity; an early in vitro identification of phototoxic potential of new drug entities in drug discovery and development. *Curr Drug Saf* 4:123–136.

Onoue S, Seto Y, Kato M, Aoki Y, Kojo Y, and Yamada S (2013b) Inhalable powder formulation of pirfenidone with reduced phototoxic risk for treatment of pulmonary fibrosis. *Pharm Res* 30: 1586–1596.

Onoue S and Tsuda Y (2006) Analytical studies on the prediction of photosensitive/phototoxic potential of pharmaceutical substances. *Pharm Res* 23:156–164.

Onoue S, Yamauchi Y, Kojima T, Igarashi N, and Tsuda Y (2008b) Analytical studies on photochemical behavior of phototoxic substances; effect of detergent additives on singlet oxygen generation. *Pharm Res* 25:861–868.

Organization for Economic Cooperation and Development (OECD) (2004) OECD Guideline for Testing of Chemicals, 432, In Vitro 3T3 NRU Phototoxicity Test, OECD, Paris. http://ntp.niehs.nih.gov/iccvam/SuppDocs/FedDocs/OECD/OECDtg432.pdf

Piérard GE and Piérard-Franchimont C (1993) Dihydroxyacetone test as a substitute for the dansyl chloride test. *Dermatology* 186:133–137.

Roberts WC (1989) Safety of fenofibrate–US and worldwide experience. *Cardiology* 76: 169–179.

Seto Y, Hosoi K, Takagi H, Nakamura K, Kojima H, Yamada S, and Onoue S (2012) Exploratory and regulatory assessments on photosafety of new drug entities. *Curr Drug Saf* 7:140–148.

Seto Y, Inoue R, Kato M, Yamada S, and Onoue S (2013b) Photosafety assessments on pirfenidone: photochemical, photobiological, and pharmacokinetic characterization. *J Photochem Photobiol B* 120:44–51.

Seto Y, Inoue R, Ochi M, Gandy G, Yamada S, and Onoue S (2011) Combined use of in vitro phototoxic assessments and cassette dosing pharmacokinetic study for phototoxicity characterization of fluoroquinolones. *AAPS J* 13:482–492.

Seto Y, Kato M, Yamada S, and Onoue S (2013a) Development of micellar reactive oxygen species assay for photosafety evaluation of poorly water-soluble chemicals. *Toxicol In Vitro* 27: 1838–1846.

Seto Y, Onoue S, and Yamada S (2009) In vitro/in vivo phototoxic risk assessments of griseofulvin based on photobiochemical and pharmacokinetic behaviors. *Eur J Pharm Sci* 38: 104–111.

Spielmann H, Balls M, Dupuis J, Pape WJ, Pechovitch G, de Silva O, Holzhütter HG, Clothier R, Desolle P, and Gerberick F, et al. (1998) The International EU/COLIPA In Vitro Phototoxicity Validation Study: results of phase II (blind trial). Part I: the 3T3 NRU phototoxicity test. *Toxicol In Vitro* 12:305–327.

Spielmann H, Gerner I, Kalweit S, Moog R, Wirnsberger T, Krauser K, Kreiling R, Kreuzer H, Lüpke NP, and Miltenburger HG, et al. (1991) Interlaboratory assessment of alternatives to the Draize eye irritation test in Germany. *Toxicol In Vitro* 5:539–542.

Taketani M, Shii M. Ohura K, Ninomiya S, and Imai T (2007) Carboxylesterase in the liver and small intestine of experimental animals and human. *Life Sci* 81:924–932.

Vargas F, Canudas N, Miranda MA, and Boscá F (1993) Photodegradation and in vitro phototoxicity of fenofibrate, a photosensitizing anti-hyperlipoproteinemic drug. *Photochem Photobiol* 58:471–476.

Weil A, Caldwell J, and Strolin-Benedetti M (1988) The metabolism and disposition of fenofibrate in rat, guinea pig, and dog. *Drug Metab Dispos* 16:302–309.

Weil A, Caldwell J, and Strolin-Benedetti M (1990) The metabolism and disposition of 14C-fenofibrate in human volunteers. *Drug Metab Dispos* 18:115–120.

Westerhof W, van Hasselt BA, and Kammeijer A (1986) Quantification of UV-induced erythema with a portable computer controlled chromameter. *Photodermatol* 3:310–314.

Wójcikowski J, Boksa J, and Daniel WA (2010) Main contribution of the cytochrome P450 isoenzyme 1A2 (CYP1A2) to N-demethylation and 5-sulfoxidation of the phenothiazine neuroleptic chlorpromazine in human liver–A comparison with other phenothiazines. *Biochem Pharmacol* 80:1252–1259.

Yun HY, Joo Lee E, Youn Chung S, Choi SO, Kee Kim H, Kwon JT, Kang W, and Kwon KI (2006) The effects of food on the bioavailability of fenofibrate administered orally in healthy volunteers via sustained-release capsule. *Clin Pharmacokinet* 45:425–432.

Address correspondence to: Satomi Onoue, Department of Pharmacokinetics and Pharmacodynamics, School of Pharmaceutical Sciences, University of Shizuoka, 52-1 Yada, Suruga-ku, Shizuoka 422-8526, Japan. E-mail: onoue@u-shizuoka-ken.ac.jp

1521-0103/354/2/195–202$25.00
THE JOURNAL OF PHARMACOLOGY AND EXPERIMENTAL THERAPEUTICS

http://dx.doi.org/10.1124/jpet.115.223644
J Pharmacol Exp Ther 354:195–202, August 2015

The Journal of PHARMACOLOGY And Experimental Therapeutics

Phototoxic Risk Assessments on Benzophenone Derivatives: Photobiochemical Assessments and Dermal Cassette-Dosing Pharmacokinetic Study

Yoshiki Seto, Hiroto Ohtake, Masashi Kato, and Satomi Onoue

Department of Pharmacokinetics and Pharmacodynamics, School of Pharmaceutical Sciences, University of Shizuoka, Shizuoka, Japan

Received February 13, 2015; accepted May 21, 2015

ABSTRACT

This study aimed to qualify photosafety screening on the basis of photochemical and pharmacokinetic (PK) data on dermally applied chemicals. Six benzophenone derivatives (BZPs) were selected as model compounds, and in vitro photochemical/phototoxic characterization and dermal cassette-dosing PK study were carried out. For comparison, an in vivo phototoxicity test was also conducted. All of the BZPs exhibited strong UVA/UVB absorption with molar extinction coefficients of over 2000 $M^{-1} \times cm^{-1}$, and benzophenone and ketoprofen exhibited significant reactive oxygen species (ROS) generation upon exposure to simulated sunlight (about 2.0 mW/cm^2); however, ROS generation from sulisobenzone and dioxybenzone was negligible. To verify in vitro phototoxicity, a 3T3 neutral red uptake phototoxicity test was carried out, and benzophenone and ketoprofen were categorized to be phototoxic chemicals. The dermal PK parameters of ketoprofen were indicative of the highest dermal distribution of all BZPs tested. On the basis of its in vitro photochemical/phototoxic and PK data, ketoprofen was deduced to be highly phototoxic. The rank of predicted phototoxic risk of BZPs on the basis of the proposed screening strategy was almost in agreement with the results from the in vivo phototoxicity test. The combined use of photochemical and cassette-dosing PK data would provide reliable predictions of phototoxic risk for candidates with high productivity.

Introduction

Drug-induced phototoxicity is caused after exposure of light-exposed tissues to topically and/or systemically administered chemicals, including pharmaceuticals, cosmetics, and food ingredients, followed by exposure to sunlight, consisting of UVB (290–320 nm), UVA (320–400 nm), and UV-visible light (400–700 nm) (Moore, 1998, 2002; Onoue et al., 2009). Recently, interest in phototoxic events due to photoreactive substances has markedly increased owing to high-intensity UV rays from the sun reaching the Earth's surface upon the destruction of the ozone layer (Onoue et al., 2009). Perceptible adverse events would leave patients and consumers with negative impressions of products, and the pharmaceutical and cosmetic industries have struggled to predict and/or avoid phototoxic events. In the early 2000s, regulatory agencies, including the Food and Drug Administration, the European Medicines Agency, and the Organization for Economic Cooperation and Development (OECD), established guidance on photosafety testing of medicinal products (EMEA/CPMP, 2002, 2008; FDA/CDER, 2002; OECD, 2004). In 2014, the International Conference on Harmonization of Technical Requirements for Registration of Pharmaceuticals for Human Use (ICH) established the ICH S10 guideline (ICH, 2014), and this guidance describes photosafety assessment strategies on the basis of photochemical/photobiological properties and in vivo pharmacokinetic (PK) behaviors in UV-exposed tissues, such as skin and eyes.

Over the past few years, a number of efforts have been made to develop effective phototoxic assessments, and analytical and biochemical methodologies for evaluating phototoxic risk have been proposed, including in silico prediction models, photochemical screening tools, and in vitro phototoxicity assessments (Seto et al., 2012). In particular, UV-visible measurement (Henry et al., 2009), 3T3 neutral red uptake phototoxicity test (3T3 NRU PT) (Spielmann et al., 1994), and/or reactive oxygen species (ROS) assay (Onoue and Tsuda, 2006; Onoue et al., 2008) are currently described as recommended methodologies for evaluating the photosafety of test substances, and these photosafety assessment tools are also useful in the early stages of product development.

This work was supported in part by a Health Labour Sciences Research Grant from the Ministry of Health, Labour, and Welfare, Japan [H25-iyaku-wakate-024]; a grant from the Cosmetology Research Foundation [527]; and a grant from the Hoyu Science Foundation [31].
dx.doi.org/10.1124/jpet.115.223644.

ABBREVIATIONS: 3T3 NRU PT, 3T3 neutral red uptake phototoxicity test; BZ, benzophenone; BZP, benzophenone derivative; DMSO, dimethylsulfoxide; DO, dioxybenzone; EM, erythromycin; ESI-MS, electrospray ionization mass spectrometry; ICH, International Conference on Harmonization of Technical Requirements for Registration of Pharmaceuticals for Human Use; KT, ketoprofen; MEC, molar extinction coefficient; MRT, mean residence time; MX, mexenone; NaPB, sodium phosphate buffer; OECD, Organization for Economic Cooperation and Development; OX, oxybenzone; PIF, photoirritancy factor; PK, pharmacokinetic; QN, quinine HCl; ROS, reactive oxygen species; SB, sulisobenzone; UPLC, ultra-performance liquid chromatography.

Although effective in vitro photosafety assessments have been developed on the basis of photochemical/photobiological mechanisms, the data obtained from these methodologies cannot fully reveal the occurrence of phototoxic events in a clinical context due to a lack of data on distribution and retention in UV-exposed tissues. Previously, combined use of in vitro photochemical/phototoxic data and in vivo PK behaviors was proposed for evaluating the in vivo phototoxic risk of chemicals (Seto et al., 2009), and a cassette-dosing PK study was employed with the aim of reducing the use of research resources and enhancing throughput (Seto et al., 2011; Onoue et al., 2014a). In these previous studies, the predicted in vivo phototoxic risk of systemically exposed chemicals on the basis of the in vitro photochemical/photobiological and in vivo PK data exhibited a strong association with clinical phototoxicity findings (Seto et al., 2011; Onoue et al., 2014a). In contrast, the proposed screening strategy has not been applied to phototoxic risk assessment on dermally applied chemicals, the phototoxicity of which may lead to a no-go decision in product development.

The present study aimed to clarify the applicability of the photosafety screening using photochemical and PK data for dermally administered chemicals. Six benzophenone (BZ) derivatives (BZPs), namely, BZ, dioxybenzone (DO), ketoprofen (KT), mexenone (MX), oxybenzone (OX), and sulisobenzone (SB), were selected as model chemicals (Fig. 1). The phototoxic skin reactions by KT, MX, and OX have been reported on the basis of the results from human photopatch tests (Chuah et al., 2013; Infante Hernando et al., 2013), although these are directly applied to the skin. OX, SB, DO, and MX were developed as sunscreens (Darvay et al., 2001; Baughman et al., 2009), and KT is one of the most well known nonsteroidal anti-inflammatory drugs given via the dermal route. In this investigation, UV spectral analysis and ROS assay were carried out to evaluate the photochemical properties of BZPs, and 3T3 NRU PT was also undertaken to verify the in vitro phototoxicity of BZPs. Cassette-dosing PK study in rats after the dermal coadministration of BZPs was conducted to determine the PK behaviors of BZPs in the skin, and the skin concentration of BZPs was assessed by ultra-performance liquid chromatography equipped with electrospray ionization mass spectrometry (UPLC/ESI-MS). On the basis of the obtained in vitro photochemical/photobiochemical and in vivo dermal PK data, the in vivo phototoxic risk of the tested BZPs was rated. To compare the predicted in vivo phototoxic risk with the in vivo phototoxic observations, in vivo phototoxicity tests were also performed on each BZP.

Materials and Methods

Chemicals

BZ was purchased from Junsei Chemical (Tokyo, Japan). DO, KT, MX, OX, erythromycin (EM), dimethylsulfoxide (DMSO), imidazole, nitroblue tetrazolium, *p*-nitrosodimethylaniline, propylene glycol, disodium hydrogen phosphate 12-water, and sodium dihydrogen phosphate dihydrate were obtained from Wako Pure Chemical Industries (Osaka, Japan). Quinine HCl (QN) and SB were purchased from Sigma-Aldrich Japan (Tokyo, Japan). Acetonitrile was obtained from Honeywell International (Morristown, NJ).

UV-Visible Spectral Analysis

Each chemical was dissolved in 20 mM sodium phosphate buffer (NaPB; pH 7.4) at a final concentration of 20 μM. UV-visible absorption spectra were recorded with a Hitachi U-2010 spectrophotometer (Hitachi, Tokyo, Japan) interfaced to a PC for data processing (Spectra Manager; JASCO, Easton, MD). A spectrofluorimeter quartz cell with 10 mm path length was employed.

ROS Assay

Irradiation Conditions. Chemicals were stored in an Atlas Suntest CPS$^+$ solar simulator (Atlas Material Technology, Chicago, IL) equipped with a xenon arc lamp (1500 W) and cooling unit SR-P20FLE (Hitachi). A UV special filter (56052371; Atlas Material Technology) was installed to adapt the spectrum of the artificial light source to natural daylight, and the Atlas Suntest CPS series had a high irradiance capability that met CIE85/1989 daylight simulation requirements. The irradiation test was carried out at 25°C with irradiance of approximately 2.0 mW/cm^2, as determined using the calibrated UVA detector Dr. Hönle 0037 (Dr. Hönle, Munich, Germany).

Assay Procedure. For the detection of both singlet oxygen and superoxide generation from irradiated compounds, the ROS assay was carried out according to the validated protocol with minor modification (Onoue et al., 2013, 2014b). Briefly, each tested compound was dissolved in DMSO at 10 mM for stock solution. For the determination of singlet oxygen generation, compounds (200 μM), *p*-nitrosodimethylaniline (50 μM), and imidazole (50 μM) were dissolved in 20 mM NaPB (pH 7.4).

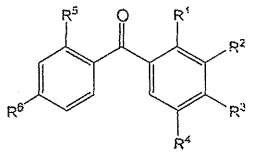

BZPs	CAS No.	Clog*P* [a]	R^1	R^2	R^3	R^4	R^5	R^6
Benzophenone (BZ)	119-61-9	3.18	–H	–H	–H	–H	–H	–H
Dioxybenzone (DO)	131-53-3	3.49	–OH	–H	$-OCH_3$	–H	–OH	–H
Ketoprofen (KT)	22071-15-4	2.76	–H		–H	–H	–H	–H
Mexenone (MX)	1641-17-4	4.08	–OH	–H	$-OCH_3$	–H	–H	$-CH_3$
Oxybenzone (OX)	131-57-7	3.59	–OH	–H	$-OCH_3$	–H	–H	–H
Sulisobenzone (SB)	4065-45-6	0.80	–OH	–H	$-OCH_3$	$-SO_3H$	–H	–H

Fig. 1. Chemical structure of tested BZPs. [a]Clog *P* calculated using ChemBioDraw Ultra 13.0 software.

To monitor the generation of superoxide, compounds (200 μM) and nitroblue tetrazolium (50 μM) were dissolved in 20 mM NaPB (pH 7.4). Each sample was mixed in a tube, and then a 200 μl sample was transferred into a well of a plastic 96-well microplate (clear, untreated, flat-bottomed; Asahi Glass, Tokyo, Japan). The samples were checked for precipitation before irradiation, and the plate fixed in the reaction container with a quartz cover was irradiated with simulated sunlight for 60 minutes. Before and after irradiation, absorbance levels at 440 nm and 560 nm were measured using SAFIRE (TECAN, Männedorf, Switzerland) for determination of singlet oxygen and superoxide generation, respectively.

3T3 NRU PT

The in vitro 3T3 NRU PT was carried out as described in the OECD test guidelines 432 with minor modification (OECD, 2004). Briefly, Balb/c 3T3 cells were maintained in culture for 24 hours for the formation of monolayers. Two 96-well plates per test chemical were then preincubated with six different concentrations of the chemical dissolved in Earle's balanced salt solution for 1 hour in duplicate. One plate was then exposed to a dose of 5 J/cm^2 UVA (+Irr experiment), whereas the other plate was kept in the dark by covering it with aluminum foil (−Irr experiment). UVA irradiation was performed using a sol 500 Sun simulator (Dr. Hönle) equipped with a 500 W metal halide lamp and a H-1 filter to remove potentially cytotoxic UVB wavelengths. The treatment medium was then replaced with culture medium and, after 24 hours, cell viability was determined by neutral red uptake for 3 hours. After that, cells were lysed in eluate (ethanol:water:acetic acid, 50:49:1), and the neutral red uptake was measured at the absorbance of 540 nm using the Benchmark Plus microplate spectrophotometer (Bio-Rad, Hercules, CA). Cell viability obtained with each of the six concentrations of the test chemical was compared with that of untreated controls, and the percent inhibition was calculated. For evaluating in vitro phototoxicity, the concentration responses obtained in the presence and in the absence of UVA irradiation were compared, usually at the IC_{50} level, that is, the concentration inhibiting cell viability by 50% compared with that of untreated controls. The photoirritancy factor (PIF) was determined using the following equation:

$$PIF = \frac{IC_{50}(-Irr)}{IC_{50}(+Irr)}.$$

In Vivo Preparation

Male Sprague-Dawley rats at 10–12 weeks of age (approximately 309–440 g body weight) were purchased from SLC (Hamamatsu, Japan), housed in the laboratory with free access to food and water, and maintained on a 12-hour dark/light cycle in a room with controlled temperature (24 ± 1°C) and humidity (55 ± 5%). On the day before experiments, rats were anesthetized with pentobarbital Na (50 mg/kg), and then the hair on the abdomen was shaved (5 cm × 5 cm). All of the procedures used in the present study were conducted according to the guidelines approved by the Institutional Animal Care and Ethical Committee of the University of Shizuoka.

Skin Deposition of BZPs after Dermal Coadministration

A cocktail solution containing all six BZPs (final concentration of each: 1 mg/ml) was prepared with the use of propylene glycol and applied to the rat skin over the abdomen (0.1 mg/rat each, $n = 5$) using an adhesive plaster for a patch test (Libatape Pharmaceutical, Kumamoto, Japan) under anesthesia with pentobarbital Na (50 mg/kg). At the indicated times (2, 4, 6, 8, 12, and 24 hours) after the dermal coadministration of BZPs, rats were humanely killed by taking blood from the descending aorta under anesthesia with pentobarbital Na (50 mg/kg), and the tissues were then perfused with cold saline from the aorta. The skin was dissected, minced with scissors, and homogenized using Physcotron (Microtec, Chiba, Japan) in 4 ml acetonitrile. After sonication for 10 minutes and shaking for 10 minutes, the samples were centrifuged (3000 rpm, 10 minutes). Extraction was repeated twice with acetonitrile, and the supernatants were pooled. The collected eluents were pooled with acetonitrile extracts, and the samples were evaporated to dryness under a gentle stream of nitrogen at 45°C. The residues were dissolved in 50% acetonitrile, including fenofibric acid (500 ng/ml) as an internal standard for UPLC analysis.

UPLC Analysis

The concentration of BZPs in rat skin was determined by UPLC/ESI-MS analysis. The UPLC/ESI-MS system consisted of a Waters Acquity UPLC system (Waters, Milford, MA), which included a binary solvent manager, a sample manager, a column compartment, and a micromass SQ detector connected with Waters Masslynx, version 4.1. A Waters Acuity UPLC BEH C18 (particle size: 1.7 μm and column size: Φ2.1 × 50 mm; Waters) was used, and the column temperature was maintained at 40°C. The standards and samples were separated using a gradient mobile phase consisting of Milli-Q containing 0.1% formic acid (A) and acetonitrile (B). The gradient conditions of the mobile phase were 0–1 minute, 50% B; 1–3 minutes, 50–75% B (linear gradient curve); 3–4 minutes, 75–95% B (linear gradient curve); 4–5.5 minutes, 95% B; and 5.5–6 minutes, 50% B, and the flow rate was set at 0.25 ml/min. Analysis was carried out using selected ion recording for specific m/z 183.2 for BZ $[M + H]^+$, 255.2 for KT $[M + H]^+$, 229.2 for OX $[M + H]^+$, 307.1 for SB $[M - H]^-$, 245.2 for DO $[M + H]^+$, 243.3 for MX $[M + H]^+$, and 319.2 for fenofibric acid $[M + H]^+$ as an internal standard. Peaks for BZ, KT, OX, SB, DO, MX, and fenofibric acid were detected at retention times of 1.96, 1.14, 2.54, 0.57, 2.54, 3.18, and 2.00, respectively. The newly developed UPLC/ESI-MS method for the determination of BZPs was validated in terms of linearity, accuracy, and precision according to the ICH guidelines "Q2B Validation of Analytical Procedures: Methodology." On the basis of the skin concentration obtained, PK analysis was performed, and the area under concentration versus time curve from 0 to 24 hours and mean residence time (MRT) were estimated using a trapezoid formula.

In Vivo Phototoxicity Testing

Each BZP or control (QN and EM) was dissolved in DMSO at 100 mg/ml and was applied to two application sites on rat skin at the abdomen (10 mg/site, $n = 4–5$) using filter paper (2 cm × 2 cm) under anesthesia with pentobarbital Na (50 mg/kg). The exposure time before irradiation was set at 3 hours after dermal administration to avoid a long time of restraint and to reduce the risk of death by supplemental anesthesia. At 3 hours after dermal administration, the filter papers containing chemicals on the application sites were removed and wiped using cotton soaked with distilled water. Then rats were irradiated individually using black light (FL15BL-B; National, Tokyo, Japan) as a UVA light source with an irradiance of approximately 2.7 mW/cm^2 for about 3 hours until the UV irradiance level reached 30 J/cm^2. Because UVB light is highly cytotoxic, a UVA light source was employed for the in vivo phototoxicity testing. During the UVA irradiation, rats were restrained on a sunbed under anesthesia with pentobarbital Na (50 mg/kg) to ensure uniform irradiation of their abdomen, and nonirradiated sites were wrapped in aluminum foil for protection from UV rays. UV intensity was monitored using the calibrated UVA detector Dr. Hönle 0037. A colorimeter equipped with a data processor (NF333; Nippon Denshoku, Tokyo, Japan) was used as a measure of skin color. This instrument records three-dimensional color reflectance, so-called $L^*a^*b^*$ system, as recommended by the Commission Internationale de l'Eclairage. The luminance (L^*) gives the relative brightness ranging from total black ($L^* = 0$) to total white ($L^* = 100$). The hue (a^*) axis represents the balance between red (positive values up to 100) and green (negative values up to −100), and the chroma (b^*) axis

represents the balance between yellow (positive values up to 100) and blue (negative values up to −100). The differences in skin color (ΔE) between before and after irradiation were described as follows (Westerhof et al., 1986; Pierard and Pierard-Franchimont, 1993):

$$\Delta E = \sqrt{(\Delta L^*)^2 + (\Delta a^*)^2 + (\Delta b^*)^2}.$$

Data Analysis

For statistical comparisons, one-way analysis of variance with pairwise comparison by Fisher's least significant difference procedure was used. A P value of less than 0.05 was considered significant for all analyses. Theoretical calculations of the lipophilicity as calculated log P (Clog P) were performed using ChemBioDraw Ultra 13.0 (PerkinElmer, Waltham, MA) with chemical structure inputs.

Results

Photochemical Characterization of BZPs. As a first step of phototoxic events, phototoxic compounds are transferred from their ground state to an excited state by absorption of photon energy from sunlight, and UV-visible spectral analysis in the range of 290–700 nm is recommended by guidelines as a rapid and simple method for predicting the photoreactive/phototoxic potential of chemicals (Seto et al., 2012). Thus, the UV-visible spectral patterns of six BZPs (20 μM) were recorded in 20 mM NaPB (pH 7.4). All BZPs exhibited intense absorption in the UVA/B range (Fig. 2A); in contrast, absorption spectral patterns of BZPs could not be observed in the visible light region (data not shown). On the basis of the spectral patterns obtained, molar extinction coefficient (MEC) values of BZPs at 290 nm were calculated as follows: 2317 (BZ), 10,833 (DO), 4350 (KT), 2850 (MX), 6817 (OX), and 11,700 (SB) $M^{-1}\cdot cm^{-1}$. According to the previous report (Henry et al., 2009) and ICH S10 photosafety guidance (ICH, 2014), compounds with MEC values greater than 1000 $M^{-1}\cdot cm^{-1}$ at any wavelength (290–700 nm) are considered to be of greater photosafety risk. In this study, all tested BZPs were thus suggested to have photoexcitability and photoreactive potential, possibly leading to phototoxic reactions.

In the indirect process of phototoxic events, ROS, including singlet oxygen and superoxide, are well known as principal intermediate species, and oxidative damage against biomolecules by chemicals after sunlight exposure mainly arises via ROS, resulting in various phototoxic events (Epstein, 1983). Thus, monitoring ROS generation from photoirradiated chemicals would be useful for evaluating the phototoxic risk of chemicals. To clarify the photoreactivity of BZPs, the ROS assay was undertaken with the use of six BZPs at 200 μM, and QN and EM (200 μM) were employed as positive and negative controls for ROS generation, respectively (Fig. 2B). KT and QN exhibited significant generation of both singlet oxygen and superoxide under simulated sunlight exposure, and BZ and OX yielded singlet oxygen via a type II photochemical reaction. In contrast, ROS generation from DO, SB, and EM was negligible, and the ROS data on MX could not be obtained owing to the appearance of precipitation of MX. As for poorly water-soluble chemicals, a lower concentration of chemicals can be applied to the ROS assay for evaluating photoreactivity; therefore, for further investigation, ROS assay on MX at 100 μM was also carried out. The generation of singlet oxygen from irradiated MX could be detected without the precipitation of MX ($\Delta A_{440\ nm}\cdot 10^3$: 67), whereas the generation of superoxide anion from irradiated MX (100 μM) was negligible. The chemicals can be determined to be photoreactive if the obtained ROS data surpass the previously defined criteria in the ROS assay [singlet oxygen ($\Delta A_{440\ nm}\cdot 10^3$): 25; and superoxide ($\Delta A_{560\ nm}\cdot 10^3$): 20] (Onoue et al., 2008, 2014b). On the basis of these criteria, BZ, KT, MX, and OX were found to be photoreactive, and these BZPs would cause phototoxic reactions in the skin. DO and SB were judged to be less photoreactive by ROS assay, whereas, interestingly, their MEC values were higher than those of the other BZPs generating ROS. These findings might suggest that UV-visible absorption properties would not always reflect the rank-order photoreactivity/phototoxicity of chemicals.

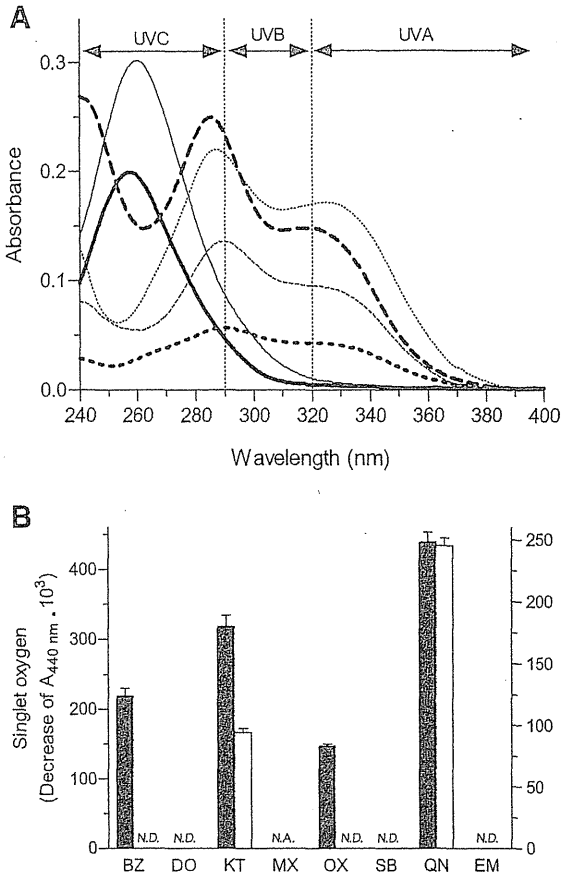

Fig. 2. In vitro photochemical properties of BZPs. (A) UV absorption spectra of BZPs (20 μM) in 20 mM NaPB (pH 7.4). Thick solid line, BZ; thin solid line, KT; thin dashed line, OX; thick dashed line, SB; thin dotted line, DO; and thick dotted line, MX. (B) Generation of singlet oxygen (filled bars) and superoxide (open bars) from BZPs (200 μM) exposed to simulated sunlight (about 2.0 mW/cm^2). QN and EM as positive and negative controls, respectively. Data represent mean ± SD for three experiments. N.A., not applicable; N.D., not detected.

In Vitro Phototoxicity of BZPs. For evaluating in vitro phototoxicity, 3T3 NRU PT, which is widely used as an alternative in vitro methodology to various in vivo photosafety assessments, was conducted. The 3T3 NRU PT was developed and validated under the auspices of European Centre for the Validation of Alternative Methods from 1992 to 1997 (Liebsch and Spielmann, 2002), and the OECD recommends this in vitro methodology for evaluating the photosafety of chemicals (OECD, 2004). The 3T3 NRU PT assesses the

concentration-dependent cytotoxicity on the Balb/c 3T3 mouse fibroblast cell line of UVA-irradiated chemicals using the uptake of neutral red by living cells. The cell viability curves of BZPs with or without UVA irradiation were obtained, and the PIF values were calculated (Table 1). Compared with the nonirradiated groups, UVA-irradiated BZ and KT exhibited significant cytotoxicity at lower doses, and the viability curves of UVA-irradiated groups were shifted to the left. The PIF values of BZ and KT were estimated to be 49.5 or more and 68.9, respectively. In contrast, the PIF values of DO, OX, and SB were calculated to be about 1.0 because these chemicals produced similar cell viability curves between UVA-irradiated and nonirradiated groups. The cytotoxicity of MX could not be fully monitored owing to its poor solubility to the assay mixture, and the PIF values of MX could not be calculated; therefore, 3T3 NRU PT would not be suitable for evaluating the phototoxicity of MX. According to the OECD test guidelines 432, classification criteria of 3T3 NRU PT on the basis of PIF values are defined as follows: 1) phototoxicity (PIF $\geq$ 5); 2) probable phototoxicity (2 $\leq$ PIF $<$ 5); and 3) nonphototoxicity (PIF $<$ 2) (OECD, 2004). Thus, BZ and KT were identified as phototoxic molecules, and DO, OX, and SB were determined as nonphototoxic ones.

Pharmacokinetic Behaviors of BZPs. The deposition of chemicals to sunlight-exposed tissues, including skin and eyes, was shown to be closely associated with the incidence of drug-induced phototoxic reactions (Seto et al., 2012), and the ICH S10 photosafety guidance describes in vivo PK behaviors as important factors of drug-induced phototoxicity (ICH, 2014); therefore, monitoring the skin concentration of dermally administered chemicals should be a key consideration for phototoxic risk prediction. In the present investigation, dermal cassette-dosing PK study was employed for improving the throughput of experiments and reducing the use of various research resources. In particular, considering implementation of the 3Rs principles (refinement, reduction, and replacement), cassette-dosing approaches can make a strong contribution to reducing the number of animals humanely killed (Allen et al., 1998). The concentration versus time curves in the skin after dermal coadministration of the six BZPs (0.1 mg/rat each) were obtained by UPLC/ESI-MS analysis (Fig. 3), and the PK parameters of the BZPs were also calculated on the basis of the concentration-time profiles obtained (Table 1). With regard to BZ, the skin concentration reached the maximum concentration (C_{max}) at 4 hours after dermal coadministration (about 6.1 μg/g tissue) and then decreased steadily. As for DO, MX, and OX, these three BZPs gradually increased their skin concentration, and each of their skin concentrations almost reached C_{max} by approximately 4 hours after dermal coadministration. The exposure levels of the skin to these three BZPs were maintained around each of their C_{max} until about 8 hours after dermal coadministration, and then they were eliminated from the skin. From these findings, the phototoxic risk of the three BZPs would persist for 4–8 hours. Unlike the PK behaviors of the other four BZPs, the skin depositions of KT and SB reached their C_{max} at 24 hours after dermal coadministration, and their elimination phase could not be observed under the present experimental conditions. The skin concentration of KT, in particular, remained around its C_{max} value (8.7 μg/g tissue) from 8 to 24 hours after dermal coadministration, and the area under the concentration versus time curve from 0 to 24 h and MRT of KT were estimated to be 160.0 hours·μg/g tissue and over 14.2 hours, respectively; therefore, KT would be associated with higher and longer exposure of the skin after dermal administration than the other BZPs. Previously, long skin retention of KT after dermal administration was observed in guinea pigs (Nakazawa et al., 2006), and the present outcomes are in agreement with this previous report. SB also exhibited the highest MRT value (>14.9 hours) among the tested BZPs, affecting the duration of exposure risk of the skin to SB.

In Vivo Phototoxicity on BZPs. To confirm the assessment capability of the photosafety screening, the in vivo phototoxicity of BZPs was also evaluated. In this study, in vivo phototoxicity testing in rat skin after dermal administration of each BZP, QN (positive control), and EM (negative control) at a dose of 10 mg/site was also conducted for screening purposes. On the basis of the dermal cassette-dosing PK study, most of tested BZPs reached C_{max} (BZ) or near C_{max} (DO, MX, and OX) at about 4 hours; therefore, exposure of the

TABLE 1
Decision matrix

	BZ	DO	KT	MX	OX	SB
UV-visible spectral analysis						
MEC ($M^{-1}\cdot cm^{-1}$)	2317[a]	10,833[a]	4350[a]	2850[a]	6817[a]	11,700[a]
ROS assay						
$^1O_2$ ($\Delta A_{440\ nm}\cdot 10^3$)[b]	219[a]	N.D.	318[a]	67[a,c]	147[a]	N.D.
O_2^- ($\Delta A_{560\ nm}\cdot 10^3$)[d]	N.D.	N.D.	94[a]	N.D.[c]	N.D.	N.D.
3T3 NRU PT						
PIF	49.5[a]	1.0	68.9[a]	N.A.	1.0	1.0
PK analysis after dermal coadministration[e]						
T_{max} (h)	4	6	24	8	6	24
C_{max} (μg/g tissue)	6.1 ± 0.6	6.0 ± 1.0	8.7 ± 0.9[a]	7.8 ± 0.5	7.8 ± 1.2	7.8 ± 0.5
AUC_{0-24} (h·μg/g tissue)	64.5 ± 2.8	53.4 ± 3.1	160.0 ± 7.3	87.6 ± 4.0	98.6 ± 5.1	133.5 ± 7.4
MRT (h)	8.4 ± 0.3	7.2 ± 0.3	>14.2[a]	8.4 ± 0.2	9.3 ± 0.2	>14.9[a]

AUC_{0-24}, area under the concentration versus time curve from 0 to 24 hours. N.A., not applicable due to solubility issue; N.D., not detected.

[a]High levels of each crucial factor: MEC values over 1000 $M^{-1}\cdot cm^{-1}$ in the UV-visible spectral analysis; ROS data over criteria in the ROS assay ($^1O_2$ [$\Delta A_{440\ nm}\cdot 10^3$]: 25; and O_2^- [$\Delta A_{560\ nm}\cdot 10^3$]: 20); PIF values over criteria in the 3T3 NRU PT (PIF: 5); and higher values of PK parameters (C_{max} and MRT) in the PK analysis.

[b]Decrease in $A_{440\ nm}\cdot 10^3$.

[d]Increase in $A_{560\ nm}\cdot 10^3$.

[c]ROS data from irradiated MX (100 μM).

[e]C_{max} and MRT values were used as crucial factors for in vivo phototoxic prediction. Each value represents mean ± S.E. for five rats.

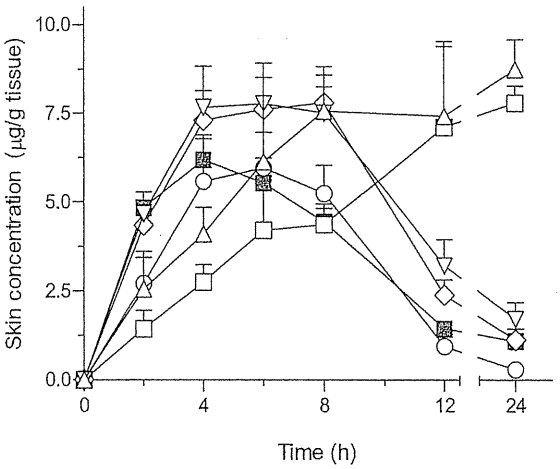

Fig. 3. Skin concentration-time profiles after dermal coadministration of BZPs (0.1 mg/rat each). ▣, BZ; △, KT; ▽, OX; □, SB; ○, DO; and ◇, MX. Data represent mean for five rats.

skin to tested BZPs for 3 hours was undertaken, and then UVA irradiation was conducted for about 3 hours in the in vivo phototoxicity test. In contrast, in the present experiment sequence, the skin deposition of KT and SB might not be sufficient for induction of phototoxicity on the basis of the obtained PK data. To avoid insufficient skin exposure to tested BZPs, the 100-fold higher doses for dermal application were employed in the in vivo phototoxicity test compared with those in the cassette-dosing PK study. UVA-induced cutaneous inflammation was monitored by changes in skin color, and skin color was measured before and after UVA irradiation using a colorimeter with the $L^*a^*b^*$ system (Fig. 4). In the $L^*a^*b^*$ system, L^* represents brightness of shade, and a^* and b^* represent the amount of red-green and yellow-blue color, respectively. In colorimetrical evaluation of the skin surface, QN was associated with a significant difference in ΔE values between irradiated and nonirradiated sites. The difference of ΔE values was calculated to be approximately 7.5 and was almost the same value as for orally administered QN in the previous in vivo phototoxicity test (Onoue et al., 2014a). In

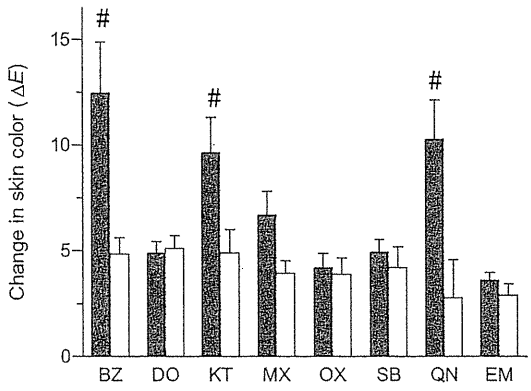

Fig. 4. Colorimetrical evaluation of skin inflammation induced by irradiated BZPs. Differences in skin color (ΔE) between before and after irradiation were estimated on the basis of L^*, a^*, and b^* values. QN and EM as positive and negative controls, respectively. Filled bars, UVA-irradiated group; open bars, nonirradiated group. Data represent mean ± S.E. of four to five rats. $^{\#}P < 0.05$, significantly different from corresponding nonirradiated group.

contrast, the difference in ΔE values of EM between irradiated and nonirradiated sites was not significant, and EM might not induce phototoxic events in the present conditions; therefore, the in vivo phototoxicity test would have been adequately carried out, and the obtained outcomes may be reliable to some extent. The ΔE values of BZ and KT in the irradiated groups were significantly different from those in the corresponding nonirradiated groups, and irradiated MX tended to exhibit a high ΔE value compared with nonirradiated MX ($P = 0.0607$). Thus, BZ and KT would have potent in vivo phototoxicity, and MX was determined to be a moderately phototoxic compound. In contrast, for DO, OX, and SB, a significant difference between the irradiated and nonirradiated groups could not be observed, and the in vivo phototoxicity of these three BZPs would be extremely low.

Discussion

In the present investigation, photosafety screening with the combined use of in vitro photochemical assessments and a dermal cassette-dosing approach was applied to in vivo phototoxicity evaluation on six dermally administered BZPs. From the present in vitro photochemical characterization, all BZPs indicated strong UV absorption on the basis of their MEC values (Henry et al., 2009); however, ROS generation from irradiated DO and SB was negligible. Referring to ICH S10 guideline, a negative result in the ROS assay supersedes a positive indication in UV-visible spectral analysis (ICH, 2014). BZ, KT, MX, and OX were found to have potent photoreactivity, possibly leading to phototoxic events in skin. By contrast, DO and SB were judged to be less phototoxic chemicals because ROS generation from irradiated DO and SB was negligible. Hence, the photoreactivity of BZPs was ranked on the basis of the present photochemical characterization as follows: KT>BZ>OX>MX≫SB≒DO. The 3T3 NRU PT was also conducted, and, on the basis of the results obtained, the rank of in vitro phototoxicity of BZPs was as follows: KT>BZ≫OX≒SB≒DO. According to the dermal cassette-dosing PK study using UPLC/ESI-MS, skin exposure levels of KT and SB were higher and lasted longer than those of the other tested BZPs, and the order for skin deposition properties on the basis of the C_{max} and MRT was determined as follows: KT>SB≫OX>MX>BZ>DO.

The ICH S10 guideline (ICH, 2014) has described the critical characteristics of a phototoxicant as follows: 1) absorption of sunlight ranging from 290 to 700 nm; 2) generation of reactive species including ROS; and 3) sufficient distribution to light-exposed tissues. The in vitro photoreactivity/phototoxicity and in vivo PK profiles in the skin were obtained as crucial factors for evaluating the in vivo cutaneous phototoxic risk of tested BZPs. To integrate these results for phototoxic risk prediction on the six BZPs tested, a decision matrix was built using the experimental outcomes, including MEC, ROS data, PIF, C_{max}, and MRT (Table 1). A decision matrix is a summarized schematic model of qualitative or quantitative data, which enables systemic identification, analysis, and evaluation of complicated sets of experimental outcomes (Seto et al., 2011). In the present decision matrix, if both in vitro photoreactivity/phototoxicity and PK profiles are high, the tested chemical is determined to have high phototoxic potential. In contrast, a low level of either of these two factors would lead to a judgment of a mild

TABLE 2
The outcomes from photosafety assessments on BZPs

	Obtained Data/Prediction										
Proposed photosafety screenings	KT	≫	BZ	>	MX	>	OX	≫	SB	≒	DO
In vivo phototoxicity test	BZ	>	KT	>	MX	≫	SB	≒	OX	≒	DO

phototoxic risk of the tested chemical. As weighting for the phototoxic prediction, in vitro photoreactivity/phototoxicity has precedence over in vivo PK profiles because photoreactivity is reported as a key trigger for phototoxic reactions (Onoue et al., 2009); therefore, low-photoreactive chemicals were determined to be less phototoxic even if their PK parameters were high. ICH S10 guideline (ICH, 2014) has described that a photoreactive chemical with longer residence time in light-exposed tissues is more likely to produce a phototoxic reaction than a photoreactive compound having a shorter residence time. On the basis of the decision matrix, KT was deduced to have the most potent phototoxic risk because of its high in vitro photoreactivity/phototoxicity and high levels of skin deposition. Additionally, long-term dermal exposure risk of KT was suspected from the MRT value, and the cutaneous phototoxic risk might persist longer. BZ would also have potent phototoxic risk owing to significant singlet oxygen generation and potent in vitro phototoxicity even though its skin deposition was low. Although the in vitro phototoxicity of MX could not be evaluated by 3T3 NRU PT because of its poor solubility, MX determined to have phototoxic risk on the basis of its high photoreactivity and moderate skin exposure. In contrast, OX was deduced to be a less phototoxic agent due to the negative outcome from the in vitro phototoxicity test even if the positive results were obtained from in vitro photochemical assessments. SB would have less phototoxic potential due to its low in vitro photoreactivity/phototoxicity, although the MRT value of SB was almost the same as that of KT. DO was also determined to be less phototoxic because its low levels of both in vitro photoreactivity/phototoxicity and in vivo PK behaviors in the skin were observed. Overall, on the basis of the decision matrix, the order for in vivo phototoxic risk of tested BZPs was deduced as follows: KT≫BZ>MX>OX≫SB≒DO (Table 2).

To clarify the in vivo phototoxicity of tested BZPs, in vivo phototoxicity test was also conducted on the six BZPs. According to the phototoxic outcomes obtained from the experiment, the ranks of phototoxicity of BZPs were as follows: BZ>KT≫MX>SB≒OX≒DO for in vivo phototoxicity (Table 2). From these findings, the order of in vivo phototoxic risk on six BZPs determined by photosafety screening was likely to show agreement with the in vivo phototoxicity of BZPs. As for MX, the 3T3 NRU PT was not applicable owing to its poorly aqueous solubility; however, the photoreactivity of MX could be obtained using the ROS assay, and in vivo phototoxic risk of MX could be deduced on the basis of the photoreactivity and dermal PK behaviors. Thus, the photoreactivity data from the ROS assay would be of help for in vivo photosafety prediction if the in vitro phototoxicity information on a chemical is not available. Phototoxic skin reactions have been divided into at least three types, namely, photoirritancy, photogenotoxicity, and photoallergy, on the basis of the mechanisms of drug-induced phototoxicity, and ROS generation from an irradiated chemical can be a key trigger for all types of phototoxic events; therefore, the ROS assay is theoretically available for evaluating the risk of all types of phototoxicity (Onoue and Tsuda, 2006). Hence, the proposed photosafety screening might be able to demonstrate all types of in vivo phototoxic risk of compounds with high accuracy, and, in the case of negative outcomes on chemicals, it would lead to the avoidance of in vivo phototoxicity test, achieving a reduction of the number of animals humanely killed.

For further investigation, Clog *P* values of BZPs were calculated using ChemBioDraw Ultra 13.0 software as an indicator of their lipophilicity (Fig. 1) because lipophilicity has been thought to be a dominant factor determining the skin permeability of dermally administered chemicals (Abraham and Ibrahim, 2007). On the basis of the Clog *P* values and the obtained concentration-time profiles in the skin, there appeared to be some relationship between lipophilicity and skin absorption behaviors of BZPs. From these findings, lipophilicity and related parameters might be useful for estimating the skin absorption properties of chemicals after dermal administration. By contrast, the prediction of the skin distribution of orally administered phenothiazines was challenging on the basis of Clog *P* values (Onoue et al., 2014a). In this study, for screening purposes, the lipophilicity and related parameters might be of help to establish an in silico approach as an alternative methodology for in vivo dermal PK study, and development of a nonanimal photosafety assessment with combined use of in silico skin permeability and in vitro photoreactivity/phototoxicity might make a major contribution to animal welfare. However, in vivo PK profiling would still be important for estimating temporal changes in the phototoxic risk of compounds, including appearance time and duration of retention.

From the present findings, the proposed photosafety screening on the basis of the in vitro photoreactive/phototoxicity and in vivo PK data could evaluate the phototoxic risk of BZPs and would be applicable to the prediction of in vivo phototoxic risk, including all types of phototoxicity, on dermally administered chemicals with high accuracy. Recently, interest in the photosafety of chemicals has increased in both regulatory agencies and industry, and regulatory agencies have recommended the implementation of the 3Rs principle (refinement, reduction, and replacement). Considering these trends surrounding product development, the proposed screening would be useful for evaluating the in vivo phototoxic risk of chemicals in product development on a large scale.

Authorship Contributions

Participated in research design: Seto, Ohtake, Kato, Onoue.
Conducted experiments: Ohtake, Kato.
Contributed new reagents or analytic tools: Seto, Ohtake, Kato, Onoue.
Performed data analysis: Seto, Ohtake, Kato, Onoue.
Wrote or contributed to the writing of the manuscript: Seto, Ohtake, Onoue.

References

Abraham MH and Ibrahim A (2007) Blood or plasma to skin distribution of drugs: a linear free energy analysis. *Int J Pharm* **329**:129–134.

Allen MC, Shah TS, and Day WW (1998) Rapid determination of oral pharmacokinetics and plasma free fraction using cocktail approaches: methods and application. *Pharm Res* **15**:93–97.

Baughman BM, Stennett E, Lipner RE, Rudawsky AC, and Schmidtke SJ (2009) Structural and spectroscopic studies of the photophysical properties of benzophenone derivatives. *J Phys Chem A* **113**:8011–8019.

Chuah SY, Leow YH, Goon AT, Theng CT, and Chong WS (2013) Photopatch testing in Asians: a 5-year experience in Singapore. *Photodermatol Photoimmunol Photomed* **29**:116–120.

Darvay A, White IR, Rycroft RJ, Jones AB, Hawk JL, and McFadden JP (2001) Photoallergic contact dermatitis is uncommon. *Br J Dermatol* **145**:597–601.

Epstein JH (1983) Phototoxicity and photoallergy in man. *J Am Acad Dermatol* **8**: 141–147.

European Agency for the Evaluation of Medicinal Products, Evaluation of Medicines for Human Use, Committee for Proprietary Medicinal Products (EMEA/CPMP) (2002) Note for Guidance on Photosafety Testing, CPMP/SWP/398/01, EMA, London.

European Agency for the Evaluation of Medicinal Products, Evaluation of Medicines for Human Use, Committee for Proprietary Medicinal Products (EMEA/CPMP) (2008) Concept Paper on the Need for Revision of the Note for Guidance on Photosafety Testing, CPMP/SWP/398/01, EMA, London.

Food and Drug Administration, Center for Drug Evaluation and Research (FDA/CDER) (2002) Guidance for Industry, in *Photosafety Testing*, FDA, Silver Springs, MD.

Henry B, Foti C, and Alsante K (2009) Can light absorption and photostability data be used to assess the photosafety risks in patients for a new drug molecule? *J Photochem Photobiol B* **96**:57–62.

Infante Hernando L, Serra-Baldrich E, Dordal T, and Puig Sanz L (2013) Photoallergic contact dermatitis caused by benzophenones in magazine inks. *Contact Dermat* **69**:124–126.

International Conference on Harmonization of Technical Requirements for Registration of Pharmaceuticals for Human Use (ICH) (2014) ICH Guideline S10 Guidance on Phototoxicity Evaluation of Pharmaceuticals, ICH, Geneva, Switzerland.

Liebsch M and Spielmann H (2002) Currently available *in vitro* methods used in the regulatory toxicology. *Toxicol Lett* **127**:127–134.

Moore DE (1998) Mechanisms of photosensitization by phototoxic drugs. *Mutat Res* **422**:165–173.

Moore DE (2002) Drug-induced cutaneous photosensitivity: incidence, mechanism, prevention and management. *Drug Saf* **25**:345–372.

Nakazawa T, Shimo T, Chikamatsu N, Igarashi T, Nagata O, and Yamamoto M (2006) Study on the mechanism of photosensitive dermatitis caused by ketoprofen in the guinea pig. *Arch Toxicol* **80**:442–448.

Onoue S and Tsuda Y (2006) Analytical studies on the prediction of photosensitive/phototoxic potential of pharmaceutical substances. *Pharm Res* **23**:156–164.

Onoue S, Kawamura K, Igarashi N, Zhou Y, Fujikawa M, Yamada H, Tsuda Y, Seto Y, and Yamada S (2008) Reactive oxygen species assay-based risk assessment of drug-induced phototoxicity: classification criteria and application to drug candidates. *J Pharm Biomed Anal* **47**:967–972.

Onoue S, Seto Y, Gandy G, and Yamada S (2009) Drug-induced phototoxicity; an early *in vitro* identification of phototoxic potential of new drug entities in drug discovery and development. *Curr Drug Saf* **4**:123–136.

Onoue S, Hosoi K, Wakuri S, Iwase Y, Yamamoto T, Matsuoka N, Nakamura K, Toda T, Takagi H, Osaki N, et al. (2013) Establishment and intra-/inter-laboratory validation of a standard protocol of reactive oxygen species assay for chemical photosafety evaluation. *J Appl Toxicol* **33**:1241–1250.

Onoue S, Kato M, Inoue R, Seto Y, and Yamada S (2014a) Photosafety screening of phenothiazine derivatives with combined use of photochemical and cassette-dosing pharmacokinetic data. *Toxicol Sci* **137**:469–477.

Onoue S, Hosoi K, Toda T, Takagi H, Osaki N, Matsumoto Y, Kawakami S, Wakuri S, Iwase Y, Yamamoto T, et al. (2014b) Intra-/inter-laboratory validation study on reactive oxygen species assay for chemical photosafety evaluation using two different solar simulators. *Toxicol In Vitro* **28**:515–523.

Organization for Economic Cooperation and Development (OECD) (2004) OECD Guideline for Testing of Chemicals, 432, In Vitro 3T3 NRU Phototoxicity Test, OECD, Paris.

Piérard GE and Piérard-Franchimont C (1993) Dihydroxyacetone test as a substitute for the dansyl chloride test. *Dermatology* **186**:133–137.

Seto Y, Onoue S, and Yamada S (2009) *In vitro*/*in vivo* phototoxic risk assessments of griseofulvin based on photobiochemical and pharmacokinetic behaviors. *Eur J Pharm Sci* **38**:104–111.

Seto Y, Inoue R, Ochi M, Gandy G, Yamada S, and Onoue S (2011) Combined use of in vitro phototoxic assessments and cassette dosing pharmacokinetic study for phototoxicity characterization of fluoroquinolones. *AAPS J* **13**:482–492.

Seto Y, Hosoi K, Takagi H, Nakamura K, Kojima H, Yamada S, and Onoue S (2012) Exploratory and regulatory assessments on photosafety of new drug entities. *Curr Drug Saf* **7**:140–148.

Spielmann H, Liebsch M, Döring B, and Moldenhauer F (1994) First results of an EC/COLIPA validation project of *in vitro* phototoxicity testing methods. *ALTEX* **11**: 22–31.

Westerhof W, van Hasselt BA, and Kammeijer A (1986) Quantification of UV-induced erythema with a portable computer controlled chromameter. *Photodermatol* **3**: 310–314.

Address correspondence to: Dr. Satomi Onoue, Department of Pharmacokinetics and Pharmacodynamics, School of Pharmaceutical Sciences, University of Shizuoka, 52-1 Yada, Suruga-ku, Shizuoka 422-8526, Japan. E-mail: onoue@u-shizuoka-ken.ac.jp

Journal of Pharmaceutical Sciences 105 (2016) 741–746

Contents lists available at ScienceDirect

Journal of Pharmaceutical Sciences

journal homepage: www.jpharmsci.org

Pharmaceutics, Drug Delivery and Pharmaceutical Technology

Photochemical Mechanism of Riboflavin-Induced Degradation of Famotidine and a Suggested Pharmaceutical Strategy for Improving Photostability

Atsushi Uchida [1, 2, *], Satomi Onoue [2], Hiroto Ohtake [2], Yoshiki Seto [2], Tsuyoshi Teramatsu [1], Tomoko Terajima [1], Toshio Oguchi [1]

[1] Department of Pharmacy, University of Yamanashi Hospital, Chuo-city, Yamanashi 409-3898, Japan
[2] Department of Pharmacokinetics and Pharmacodynamics, School of Pharmaceutical Sciences, University of Shizuoka, Suruga-ku, Shizuoka 422-8526, Japan

ARTICLE INFO

Article history:
Received 10 July 2015
Revised 18 September 2015
Accepted 24 September 2015
Available online 27 October 2015

Keywords:
ascorbic acid
famotidine
formulation
injectables
pharmacokinetics
photodegradation
reactive oxygen species
riboflavin
stabilization
UV-VIS spectroscopy

ABSTRACT

The present study aimed to clarify the mechanism of photodegradation of famotidine with riboflavin (FMT/RF), and to develop a photochemically stabilized formulation of FMT/RF. Photochemical properties of RF were characterized by UV-VIS spectral analysis, reactive oxygen species (ROS) assay, and photostability testing. Pharmacokinetic study was conducted in rats after intravenous administration of FMT (1 mg/kg) formulation containing RF (0.01 mg/kg). The UV-VIS spectral pattern of RF partly overlapped with the sunlight spectrum, and ROS generation from photoirradiated RF was remarkable; thus, RF had high photoreactive potential. In the photostability testing, after irradiation (250 W/m^2), degradation rate for FMT in FMT/RF was ca. 11-fold higher than that in FMT alone. The addition of radical scavengers to FMT/RF led to attenuated photodegradation of FMT/RF; in particular, the addition of L-ascorbic acid (vitamin C; VC) to FMT/RF showed ca. 86% inhibition of the photodegradation of FMT/RF. The pharmacokinetic study on FMT indicated that the addition of VC (1 mg/kg) to FMT/RF had no significant impact on the pharmacokinetic behavior of FMT. These findings suggest that ROS-mediated photochemical reaction would be involved in the photodegradation pathway of FMT/RF, and the complementary use of VC might be an attractive approach to improve the photostability of FMT/RF.

Introduction

In pharmaceutical therapy, patients often receive various injectable drugs simultaneously. It is possible to reduce the invasiveness to the patient by mixing up all injectable drugs and giving them in one go via one route; however, incompatibility may occur among the applied drugs.[1,2] Incompatibility sometimes induces various undesirable reactions, including precipitation, color change, drug degradation, and yield of toxic products upon covalent binding.[3] These factors might jeopardize the safety and effectiveness of intravenous drug therapies.[4] According to the clinical case, famotidine (FMT; Fig. 1a), a histamine H_2 receptor antagonist, has been used by mixing with various drugs.[5,6] Several injectable drugs, including total parenteral nutrition and potassium chloride (KCl) preparation, contain riboflavin (RF; Fig. 1b),[5,7] and RF may lead to the photodegradation of FMT even under a daylight fluorescent lamp at room temperature.[5] The attenuation of FMT potency may cause therapeutic failure for patients with gastrointestinal diseases; however, the mechanistic aspects of the photodegradation of FMT with RF (FMT/RF) are still unclear. Thus, the clarification on the mechanism of photochemical interaction between FMT and RF may be needed to take preventive measures against the photodegradation of FMT/RF. The photochemical mechanism-based prevention can provide a desired medication for the clinical use of FMT.

RF has been commonly prescribed for the treatment of avitaminosis B_2, and it is also used as a coloring agent of KCl solution in order to avoid medical accidents, including arrhythmia and cardiac arrest.[7] Because of its high photosensitivity,[8,9] irradiated RF tends to cause photooxidation of co-existing drugs. For example, irradiated RF led to the photodegradation of various drugs, including

* *Correspondence to*: Atsushi Uchida (Telephone: +81-55-273-1111; Fax: +81-55-273-6672).
E-mail address: auchida@yamanashi.ac.jp (A. Uchida).

http://dx.doi.org/10.1002/jps.24689
0022-3549/

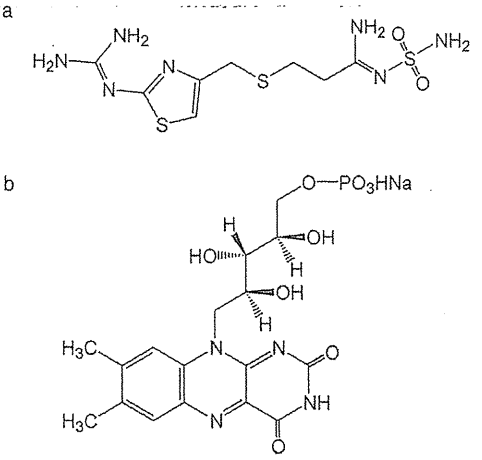

Figure 1. Chemical structures of FMT (a) and RF (b).

ceftriaxone, isoproterenol, and folate.[10-12] Reactive oxygen species (ROS)-mediated photochemical reaction may be involved in the photooxidation pathway of a drug.[13] FMT has been widely prescribed for patients with gastric ulcers, duodenal ulcers, Zollinger-Ellison syndrome, and gastroesophageal reflux disease.[14] FMT has antioxidant activity since it was shown to act as an acceptor of ROS.[15,16] From these previous observations, RF-sensitized photooxidation may be partly involved in the photodegradation pathways of FMT/RF. However, the detailed mechanisms of the photodegradation of FMT/RF have not been fully elucidated.

The present study aimed to clarify the mechanism of the photodegradation of FMT/RF in more detail. The photochemical properties of RF were characterized by UV-visible light (UV-VIS) spectral analysis and ROS assay. The degradation profile of FMT with or without RF upon irradiation was monitored, and photostability testing of FMT/RF was conducted with the addition of radical scavengers to clarify the possible involvement of a ROS-mediated mechanism in the photodegradation of FMT/RF. Furthermore, to improve the photostability of FMT/RF, a new formulation of FMT/RF was designed on the basis of the mechanisms of the photodegradation of FMT/RF. To assess the bioequivalence between FMT/RF formulations, pharmacokinetic study was carried out in rats after the intravenous administration of FMT/RF formulations.

Materials and Methods

Chemicals

FMT, RF, dimethyl sulfoxide (DMSO), imidazole, nitroblue tetrazolium (NBT), *p*-nitrosodimethylaniline (RNO), Tween 20, disodium hydrogen phosphate $12H_2O$, sodium dihydrogen phosphate dehydrate, dibutylhydroxytoluene (BHT), ammonium acetate, L-tyrosine (Tyr), sodium sulfite (Na_2SO_3), and D-mannitol were purchased from Wako Pure Chemical Industries (Osaka, Japan). Sodium azide (NaN_3), L-tryptophan (Trp), L-cysteine (Cys), and L-histidine (His) were purchased from Sigma-Aldrich Japan (Tokyo, Japan). L-Ascorbic acid (vitamin C; VC) was purchased from Nacalai Tesque, Inc. (Kyoto, Japan). Methanol (MeOH) and acetonitrile (liquid chromatography grade) were purchased from Kanto Chemical (Tokyo, Japan).

UV-VIS Spectral Analysis

FMT and RF were dissolved in 20 mM sodium phosphate buffer (NaPB) (pH 7.4) at 20 μM. UV-VIS absorption spectra were recorded with a HITACHI U-2010 spectrophotometer (HITACHI, Tokyo, Japan) interfaced to a PC for data processing (software: Spectra Manager). A spectrofluorometer quartz cell with 10-mm pathlength was employed.

ROS Assay

Irradiation Conditions

Each tested sample was stored in an Atlas Suntest CPS+ solar simulator (Atlas Material Technology LLC, Chicago, IL) equipped with a xenon arc lamp (1500 W). A UV special filter was installed to adapt the spectrum of the artificial light source to natural daylight. The irradiation tests were carried out at 25°C with an irradiance of 250 W/m^2 (300-800 nm).

Determination of ROS

The ROS assay was designed to evaluate the photochemical reactivity of the tested chemicals by determining both singlet oxygen and superoxide generated from photo-irradiated chemicals.[13,17] In the present study, the ROS assay was undertaken to clarify the photoreactivities of FMT and RF. Briefly, FMT and RF were dissolved in DMSO and 20 mM NaPB (pH 7.4), respectively. Singlet oxygen was measured by spectrophotometrically monitoring the bleaching of RNO at 440 nm using imidazole as a selective acceptor of singlet oxygen. Samples, containing tested compounds (50 μM), RNO (50 μM), imidazole (50 μM), and DMSO (2%, v/v) in 20 mM NaPB (pH 7.4) with Tween 20 (0.5%, v/v), were irradiated with simulated sunlight for the indicated periods (5, 10, 20, 30, 40, and 60 min), and then measured for their absorbance at 440 nm using a SAFIRE microplate spectrophotometer (TECAN, Mannedorf, Switzerland). To determine superoxide generation, samples, containing tested compounds (50 μM), NBT (50 μM), and DMSO (2%, v/v) in 20 mM NaPB (pH 7.4) with Tween 20 (0.5%, v/v), were exposed to simulated sunlight for the indicated periods (5, 10, 20, 30, 40, and 60 min), and reductions in NBT were measured by increases in absorbance at 560 nm using a SAFIRE microplate spectrophotometer.

Photostability Testing

Photodegradation Profiles of FMT/RF

FMT and RF were dissolved in 20 mM NaPB (pH 7.4). FMT (300 μM) and FMT (300 μM) containing RF (2 μM) with or without radical scavengers (500 μM), including NaN_3, VC, and BHT, in 5 mL clear glass vials were set in the Atlas Suntest CPS+ solar simulator, and irradiated with simulated sunlight for different periods (1.5, 3, 5, 10, 20, and 30 min). Each sample was diluted 100-fold, and the remaining FMT in the sample was determined with ultra-performance liquid chromatography equipped with electrospray ionization mass spectrometry (UPLC/ESI-MS) analysis. The UPLC/ESI-MS system consisted of a Waters Acquity UPLC™ system (Waters, Milford, MA), which included binary solvent manager, sample manager, column compartment, and SQD connected with Mass-Lynx software. An Acquity UPLC™ BEH C_{18} column (particle size: 1.7 μM, column size: 2.1 × 50 mm^2; Waters) was used, and column temperature was maintained at 60°C. Samples were separated using a gradient mobile phase consisting of 5 mM ammonium acetate (A) and acetonitrile (B) with a flow rate of 0.25 mL/min, and the retention time of FMT was ca. 1.9 min. The gradient conditions of the mobile phase were 0-0.5 min, 5% B; 0.5-2.5 min, 5%-20% B; and 2.5-4.0 min, 20%-95% B. Analysis was carried out using selected ion recording (SIR) for specific *m/z* 338.16 for FMT $[M+H]^+$.